

Article

# Penetration Resistance of Laacher See-tephra Andosols—Evaluating Rooting Conditions of Undisturbed and Excavated Forest Soils in SW-Germany

Julian J. Zemke , Ulli Bange, John Dellen, Ines Groh, Roxane C. A. Henn, Joshua Pöhler and Stephan Stegmann

Department of Geography, Institute for Integrated Natural Sciences, Campus Koblenz, University Koblenz-Landau, 56070 Koblenz, Germany; bange@uni-koblenz.de (U.B.); johndellen@uni-koblenz.de (J.D.); inesgroh@uni-koblenz.de (I.G.); roxanehenn@uni-koblenz.de (R.C.A.H.); jpoehler@uni-koblenz.de (J.P.); sstegmann@uni-koblenz.de (S.S.)

\* Correspondence: zemke@uni-koblenz.de; Tel.: +49-261-287-2282

Received: 21 February 2020; Accepted: 20 March 2020; Published: 23 March 2020



**Abstract:** This study discusses penetration resistance (PR) of forested Pumice-Andosol sites. PR, a key soil property influencing root growth and elongation, exerts a substantial influence on ecological site quality and tree growth. Andosols were expected to show low PR because of their unique characteristics (low bulk density, loose soil matrix). Five sites, two undisturbed and three backfilled, were sampled. The latter result from pumice excavation and were examined to quantify potential PR alterations in the aftermath of backfilling and pumice removal. Penetrologger sampling on undisturbed sites showed mean PR not exceeding 3 MPa, a literature-based, critical threshold restricting root growth, in the upper 0.80 m, indicating conditions fostering tree rooting. Backfilled sites mostly exhibited increased (>3 MPa) PR, leading to rooting restrictions even beginning at −0.21 m. Deviations from undisturbed soils range from −15.6 to +109.3% depending on depth and age of the backfilled site. Furthermore, GIS-based data interpolation helped to identify spatial PR patterns and allowed a direct comparison before/after backfilling at one site. Statistical analysis revealed significantly altered PR after backfilling, while a concluding ANOVA provided at least significant governing factors (depth, area, clay + silt content, soil organic matter), albeit with only small effect sizes.

**Keywords:** soil penetration resistance; Andosol; forest soil; rooting; backfilling; soil physical properties; Germany

## 1. Introduction

Soil penetration resistance (PR), often described as “( . . . ) the resistance of the soil to deformation ( . . . )” [1] (p. 1), is one of the governing soil physical characteristics for root growth and elongation (e.g., [1–5]). Studies looking at the correlation between PR and root growth were mainly carried out on agricultural crops (e.g., [6–12]). However, there have been studies explicitly addressing forest sites (e.g., [13–17]). Both consistently describe critical penetration resistances: 2 MPa is often considered to be a threshold for root growth and elongation. For example, ref. [2] observed root elongation rates reduced by 50% at PR = 2 MPa under laboratory conditions. In [13], the authors proved that 70% of all tree roots found in field observations at sandy, backfilled excavation sites were located in soils exhibiting a PR < 2 MPa. In soils exceeding 3 MPa, only 10% of all roots were found.

The main factors governing PR are depth, soil texture, soil organic matter (SOM) and soil moisture (SM) [18–24]. Studies point out that soil texture, particularly the sum of clay and silt percentage, is the most important soil property influencing PR [25,26]. In addition, SM plays an important role, as wet soils tend to show a better penetrability due to a higher plasticity [18,19]. There is also a direct connection between PR and soil dry bulk density (DBD), allowing a conversion between each other to a certain degree. However, Refs. [27,28] point out that one has to consider the percentage of SOM when converting, as high SOM content leads to lower DBD, even if PR stays constant.

This study focusses on Andosols originated from Laacher See Tephra (LST), which was deposited 12,960 a.B.P. (before present) in SW-Germany, with a maximum thickness of >20 m and 2–4 m in the spatial vicinity of the investigation area, approximately 20 km E of the Laacher See Volcano. Here, mostly pumice ashes and lapilli were deposited, functioning as base layer for Holocene pedogenesis [29–33]. Andosols are described as soils with noticeably low DBD and a loosely packed soil matrix, especially when there are coarse pumice particles present [34–36]. LST pumice itself exhibits low particle densities, mostly lower than  $1 \text{ g}\cdot\text{cm}^{-3}$ , caused by the porous structure due to gas cavities [37]. Therefore, drawing direct conclusions for rooting or ecological site characteristics on the basis of DBD-values is difficult, as there might be sites with low DBD (in fact caused by low particle density), but with an actually dense soil matrix inhibiting proper root growth. That is why PR is discussed in this study, as it potentially delivers a better indicator for actual rooting conditions.

Andosols, and especially those originated from ash- and lapilli-deposits, are being described as good soil for forestry use, as they show many beneficial characteristics fostering tree growth: They are soils with high water storage capacities, low DBD and low PR leading to good rooting conditions [38–41]. Yet, studies looking at Andosol PR explicitly are scarce. There are a few studies conducted in Rwanda [42], Kenya [43] and Chile [44–47]. For example, the latter report Andosol-PR <2 MPa for undisturbed pasture topsoil and >3 MPa after grazing. However, these studies focused on grazing and tilling actions, and therefore agricultural soils. An in-depth discussion for forested sites has not been conducted yet. That is why this study aims to deliver a first description of soil PR for forested Andosol sites, not only looking at the topsoil but delivering detailed datasets for the upper 0.8 m.

Apart from that, a second underlying question is the effect of excavation works conducted in the area. Local concrete industry excavates pumice on small parcels, covering merely a few hectares. After pumice excavation, the remaining soil is backfilled and a smooth surface is remodeled. While the effects of these actions have been discussed in regard to soil erosion processes before [48], consequences for PR are investigated in this study. Therefore, there are two underlying questions for this study: (a) Analyzing PR for forested Andosol-sites against the background of root growth threshold values, and (b) evaluating the short-, mid- and long-term effects of excavation and backfilling on PR compared to the initial, undisturbed state.

## 2. Materials and Methods

### 2.1. Investigation Area

Investigations took place in the forest district Bendorf, in a secondary valley of the Brexbach, a tributary of the river Rhine. The site is located approximately 20 km E of the Laacher See (Figure 1) and lies at the outer limit of one of the main ash-deposition fans of the Laacher See eruption [30]. Thickness of LST deposits is around 2–4 m, while the deposition took only place in a patchy pattern and mainly on N- and NW-exposed slopes, indicating the dominant wind direction during the eruption event.

Pumice excavation takes place, *inter alia*, at the NW-exposed slope of the investigation area. As described in Section 1, local concrete factories only excavate small lots at once, leading to a progressing excavation transversally following the pumice depositions across the slope. That is why excavated areas of different ages lie side by side along with areas that have not been excavated yet. The latter function as reference areas for undisturbed conditions, the former, however, provide the opportunity to

evaluate different post-excitation states regarding temporal distance from excavation. While younger backfilled soils may have not consolidated yet, leading to presumably lower PR, older sites may feature higher PR due to soil matrix consolidation or eventually loosening of the soil matrix caused by reestablished vegetation and rooting, therefore again leading to presumably lower PR in the topsoil.

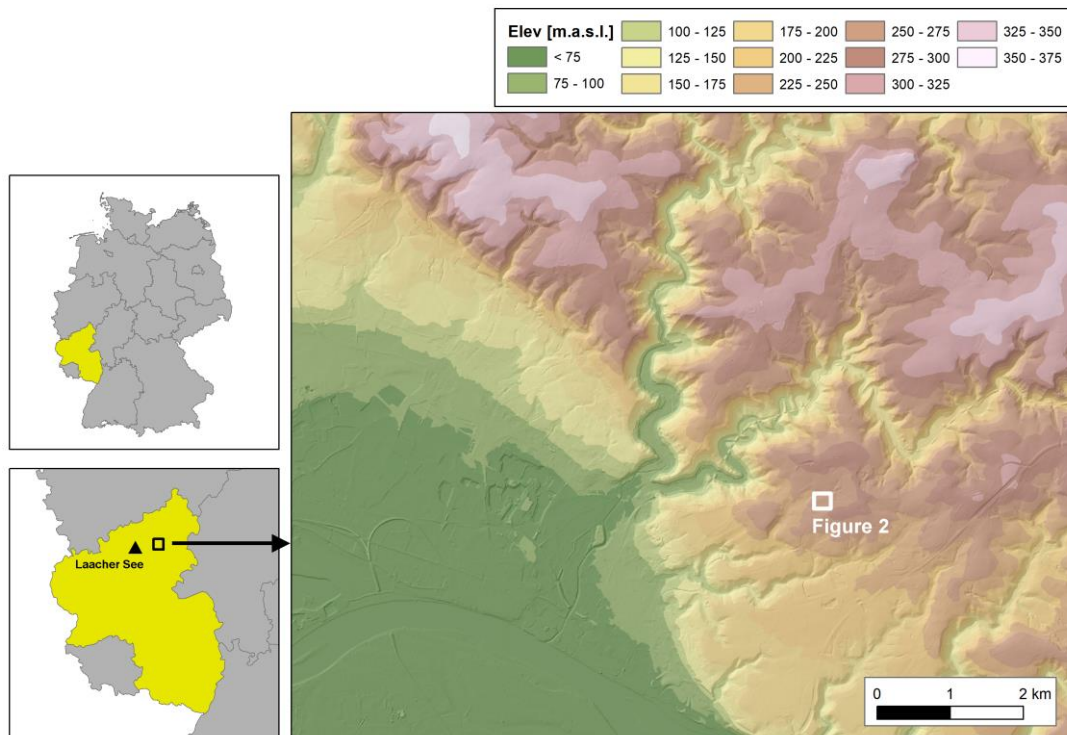


Figure 1. Location of the study area (after [37,48]).

Overall, five different sub-areas were observed in this study (Figure 2).



Figure 2. Sampling areas. Aerial photography provided by LVerGeo RLP (2019).

FOR represents the totally undisturbed state with a forest stand consisting of 70–80 a old *Fagus sylvatica*. CUT represents an undisturbed state with no excavation but already cut-down forest (*Fagus sylvatica*) in preparation for excavation in winter 2018/2019. CUT EX is the same area,

but observed in summer 2019, four months after excavation and backfilling, planted with solitary *Quercus petraea* and *Fagus sylvatica* seedlings. SUC was excavated in 2015 and already shows extensive succession vegetation in addition to *Fagus sylvatica* and *Quercus petraea* seedlings planted within. REF was excavated and reforested with dense *Betula pendula* stands and solitary *Alnus glutinosa* and *Quercus rubra* in 2002. The aerial photography in Figure 2 shows the state as in summer 2019 with an already backfilled area CUT EX. The transitional stage between CUT and CUT EX, showing excavation works, is depicted in Figure 3.



**Figure 3.** Beginning pumice excavation in forest district Bendorf, area CUT/CUT EX in late 2018 (Photo: Alexander Klein). Material for later backfilling and LST are visible on both sides. Area FOR is located on the left (West), excavation continued gradually to the right (East).

## 2.2. Sampling

Soil data was sampled in the fall of 2018 prior to this study for FOR, CUT, SUC and REF, using a variety of parameters in a soil erosion study [48]. This dataset consists of 485 individual soil samples, taken at 117 sampling points (3 catenae per area, each consisting of 10 sampling points; 3 sampling points were excluded because of corrupted data). On undisturbed sites (FOR and CUT), a horizon-wise sampling took place, while five depth-slices of 0.2 m were sampled on disturbed/backfilled sites, covering the upper first meter of the soil, as they did not have pedogenetic horizons anymore. This dataset is expanded by soil moisture measurements, which were conducted simultaneously but were not included in [48]. On CUT EX, an additional 205 samples were taken in early summer of 2019, consisting of 51 individual sampling points and again five depth classes covering 0.2 m each. These samples were also not included in [48]. Parameters used and discussed in this study are soil texture, soil moisture (SM) and soil organic matter (SOM). In order to achieve the best possible comparability between the 2018 and 2019 datasets, similar boundary conditions were sought. While soil texture and soil organic matter were defined as practically constant, soil moisture was treated as

a potentially volatile parameter. Countering this possible dataset inconsistency, climate data from weather station Grenzau (situated 2 km North of the investigation area and operated by the DLR Rhineland-Palatinate) was used to calculate an antecedent precipitation index (API) according to [49], incorporating precipitation input 21 days prior to sampling and accounting seasonality using an empirical adjustment factor. API was 0.22 mm in 2018 and 0.50 mm in 2019, showing comparable and low antecedent precipitation.

Penetration resistance was measured using an Eijkelkamp Penetrologger [28]. This device samples PR in a vertical resolution of 0.01 m from 0–0.80 m, while simultaneously locating sampling positions via built-in GPS. GPS-inaccuracies were diminished by conducting a parallel measurement with a Garmin eTrex handheld GPS using the built in point averaging method. On FOR, CUT, SUC and REF, PR was measured at 150 individual sampling points, and on CUT EX, 153 points were sampled (Figure 4).

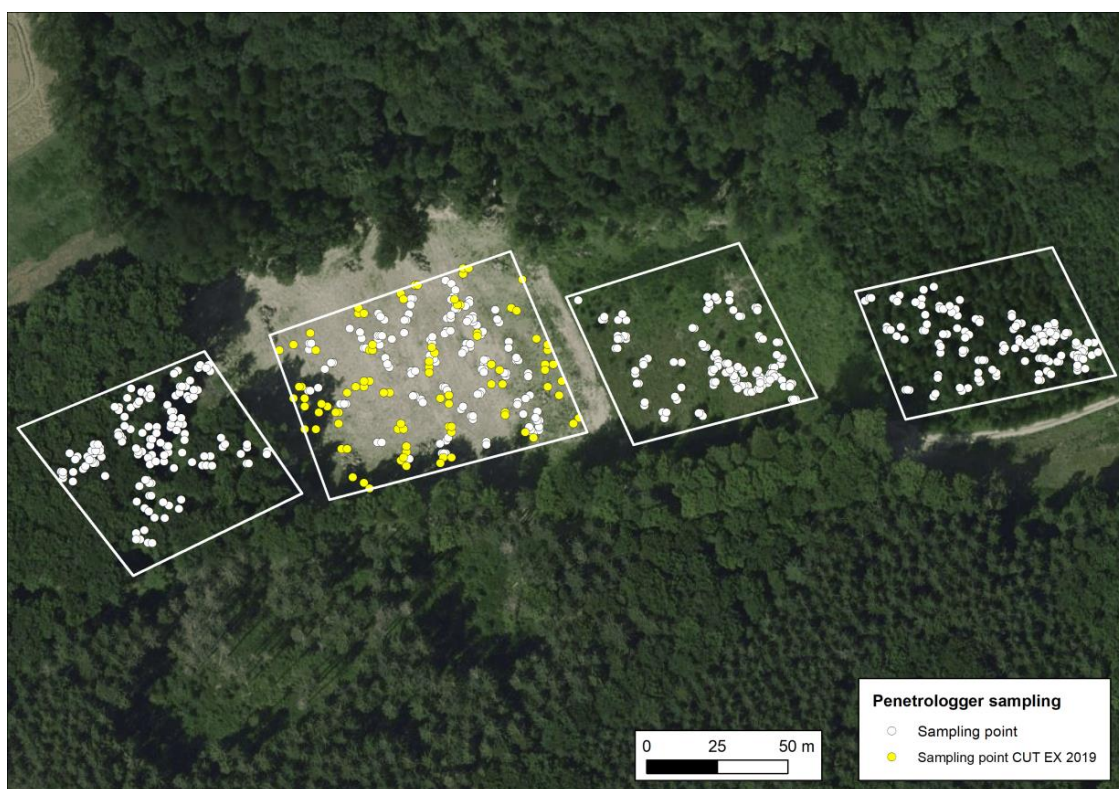


**Figure 4.** Penetrologger sampling points. Aerial photography provided by LVerGeo RLP (2019).

In order to homogenize soil and PR datasets and to simplify the detailed penetrometer dataset, all different input parameters were categorized, featuring depth-classes of 0–0.20, 0.21–0.40, 0.41–0.60 and 0.61–0.80 m. Figure 4 shows all individual penetrometer sampling points, exact soil sampling positions can be derived from [48].

### 2.3. Data Analysis and Further Statistical Analysis

Soil characteristics and PR datasets are discussed on the basis of different statistical approaches. As described, pre-collected data used in a soil erosion study in the same investigation area was combined with completely new datasets of subarea CUT EX and previously unpublished data of FOR, CUT, SUC and REF. In particular, soil texture, explicitly the sum of clay and silt (C + Si), soil moisture (SM) and soil organic matter (SOM) are discussed, as they exert an influence on PR and provide a good insight into soil structure alterations made by excavation and backfilling.

PR is the main focus of this study, which is why this dataset is discussed in-depth, beginning with a descriptive analysis against the background of PR threshold values concerning root growth.

Following up, a spatial calculation and presentation is carried out, using sampling points as input parameters for a Kriging-interpolation. Calculations were made with Golden Software Surfer (version 8), and ESRI ArcGIS 10.1 was used for visualization. Root mean square error (RMSE) was used to compare interpolated and in-situ values for every sampling point, allowing an evaluation of interpolated data quality. All spatial interpolations were carried out for every depth-slice (0–0.20, –0.21–0.40, –0.41–0.60 and –0.61–0.80 m) and with a spatial resolution of 1 × 1 m. This data analysis should provide information, if there is any sort of spatial gradient or distribution of distinctively high and/or low PR values. Additionally, area CUT EX was interpolated separately. With the help of this dataset, a direct comparison between CUT and CUT EX was possible, viewing at both absolute and relative PR changes in the aftermath of excavation and backfilling.

In addition, a deeper statistical analysis was performed, comparing sub-areas in view of their specific PR. As a first step, the Kolmogorov–Smirnov-test was conducted to check if the datasets are normally distributed. Following this, the non-parametrical Kruskal–Wallis test was used both simplified and pairwise to evaluate if there are statistical similarities between the sites. In a further step, both undisturbed sites (FOR and CUT) were aggregated to one simplified class (“Undisturbed”), allowing a better and clearer analysis of excavation-induced changes, explicitly viewing at (a) relative deviations from the undisturbed state and (b) again testing similarities using both the simplified and pairwise Kruskal–Wallis test.

Further on, a correlation analysis was carried out, testing if PR is associated with governing factors cited in existent studies. For this purpose, measuring points of PR were associated with interpolated datasets of (clay + silt), SM and SOM, as the latter provided spatially corresponding point data for each PR sampling point. As the existent literature assumes non-linear correlations between governing factors and PR [20,27,28], the Spearman correlation coefficient was calculated. Categorization of correlation strength was based on a five step rule of thumb as proposed in [50,51] (Table 1).

**Table 1.** Strength of correlation coefficients according to [50,51].

Correlation Coefficient	Strength of Correlation
0.00–(–)0.09	Negligible
(–)0.10–(–)0.39	Weak
(–)0.40–(–)0.69	Moderate
(–)0.70–(–)0.89	Strong
(–)0.90–(–)1.00	Very strong

Lastly, a multi-factorial ANOVA was carried out, testing if there are singular or combined factors that govern PR values. For this purpose, all considered factors (percentage clay and silt (C + Si), percentage SM, percentage SOM, area and depth) were converted to classified nominal datasets. While area (FOR, CUT, CUT EX, SUC, REF) and depth (interval 0.2 m) were numbered serially, class breaks were defined for the remaining factors (C + Si), SM and SOM. Breaks, and therefore class boundary values, were defined as 10, 25, 50, 75 and 90% quantile (Q<sub>10</sub>, Q<sub>25</sub>, Q<sub>50</sub>, Q<sub>75</sub>, Q<sub>90</sub>) of the dataset. Because of the rather extensive ANOVA output-table using five fixed factors, only significant ( $p < 0.05$ ) factors are presented within this study. Effect size is displayed as Cohen’s  $f$ , introduced in [52] with the categorization presented in Table 2.

**Table 2.** Effect sizes of Cohen’s  $f$  according to ([52], pp. 285–287).

$f$	Effect Size
0.10	Small
0.25	Medium
0.40	Large

All statistical analyses were performed using IBM SPSS Version 25, statistical plots were made with QtiPlot version 0.9.8.3. All featured box-plot diagrams show  $Q_{10}$  and  $Q_{90}$  as whisker,  $Q_{25}$  and  $Q_{75}$  as box boundaries and  $Q_{50}$  as a straight line within the box. Minimum, maximum and arithmetic mean appear as scatter points.

### 3. Results

#### 3.1. Soil Characteristics: Descriptive Analysis

Depth-aggregated soil texture data (Table 3) clearly indicates disturbance after excavation. Undisturbed sites (FOR, CUT) mostly show a silty loam texture in the upper 0.2 m, followed by more clayish textures. They indicate the B-Horizon, consisting of weathered tephra between  $-0.21$  and  $-0.60$  m. From  $-0.61$  m on, sandier textures were found, representing slightly weathered and unweathered tephra, addressed as (weathered) C-Horizon. In contrast, disturbed and backfilled sites mostly exhibit a noticeable majority (up to 86%) of sandy loam textures throughout all depths, indicating a thoroughly mixed soil due to backfilling, which rather represents the mean texture of the formerly separated horizons.

Besides analyzing soil texture classes, a graphical analysis was conducted to illustrate mean percentages of clay, silt and sand for each site and depth category (Figure 5).

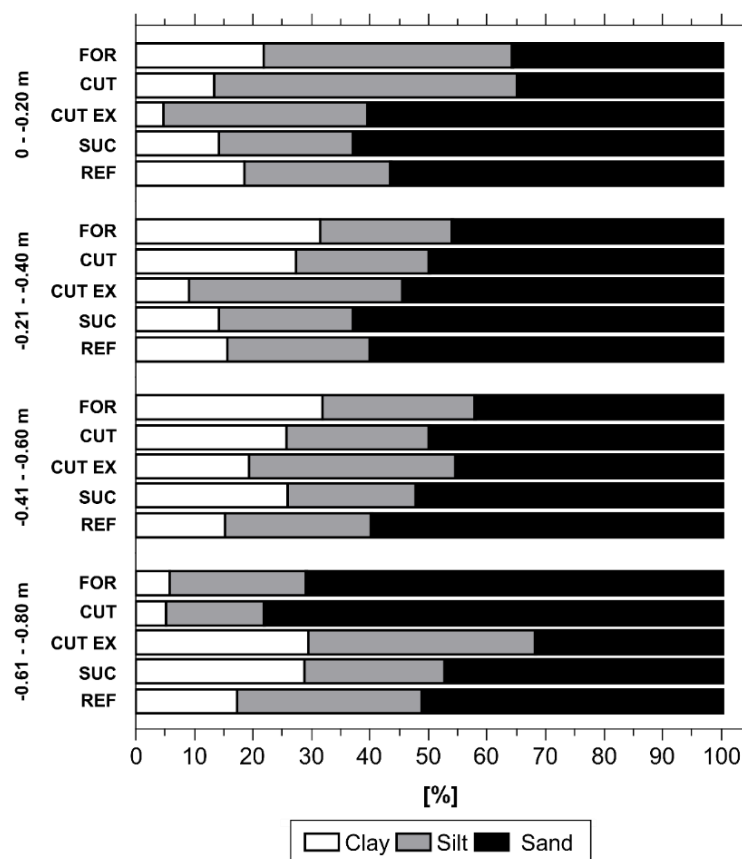


Figure 5. Mean percentages of clay, silt and sand of each area and depth-category.

**Table 3.** Soil texture percentages for depth-aggregated data, soil textures according to FAO WRB. Highest percentages indicated bold.

Depth [m]	Soil Texture	FOR	CUT	CUT EX	SUC	REF
0--0.20	S	-	-	2%	-	-
	LS	-	4%	6%	3%	10%
	SL	16%	11%	<b>86%</b>	<b>70%</b>	<b>40%</b>
	L	4%	7%	-	-	13%
	SiL	<b>56%</b>	<b>67%</b>	4%	-	7%
	Si	-	-	-	-	-
	CL	-	-	-	-	-
	SCL	8%	7%	2%	20%	13%
	SiCL	-	-	-	-	-
	SC	16%	4%	-	3%	7%
	SiC	8%	-	-	-	3%
	C	4%	-	-	3%	7%
-0.21--0.40	S	-	-	2%	-	3%
	LS	-	5%	9%	3%	3%
	SL	36%	21%	<b>73%</b>	<b>54%</b>	<b>57%</b>
	L	-	10%	2%	7%	10%
	SiL	7%	-	4%	-	7%
	Si	-	-	-	-	-
	CL	-	16%	-	-	-
	SCL	7%	16%	-	33%	10%
	SiCL	-	-	4%	-	-
	SC	7%	<b>21%</b>	2%	3%	3%
	SiC	-	-	2%	-	-
	C	<b>43%</b>	11%	2%	-	7%
-0.41--0.60	S	-	-	2%	-	3%
	LS	-	-	4%	3%	10%
	SL	20%	<b>40%</b>	<b>51%</b>	27%	<b>50%</b>
	L	-	-	4%	7%	10%
	SiL	13%	10%	7%	-	3%
	Si	-	-	-	-	-
	CL	-	10%	2%	-	-
	SCL	7%	-	4%	<b>37%</b>	13%
	SiCL	-	-	9%	3%	-
	SC	27%	30%	2%	-	7%
	SiC	-	-	2%	-	3%
	C	<b>33%</b>	10%	13%	23%	-
-0.61--0.80	S	-	18%	5%	3%	3%
	LS	31%	<b>64%</b>	2%	3%	7%
	SL	<b>69%</b>	9%	<b>24%</b>	13%	<b>50%</b>
	L	-	-	-	7%	3%
	SiL	-	-	21%	7%	3%
	Si	-	-	-	-	-
	CL	-	-	5%	-	10%
	SCL	-	9%	-	<b>33%</b>	3%
	SiCL	-	-	7%	7%	13%
	SC	-	-	7%	3%	3%
	SiC	-	-	19%	3%	-
	C	-	-	10%	20%	3%

S = Sand; LS = Loamy sand; SL = Sandy loam; L = Loam; SiL = Silty loam; Si = Silt; CL = Clay loam; SCL = Sandy clay loam; SiCL = Silty clay loam; SC = Sandy clay; SiC = Silty clay; C = Clay.

Both FOR and CUT show a similar pattern of clay-, silt- and sand-content, with dominant silt-percentages in the upper 0.2 m, indicating a well-developed A-Horizon. In all other depths, sand is the dominant grain size, with rapidly increasing percentages between -0.61 and -0.8 m, indicating only

slightly weathered or unweathered LST. Analogous to soil texture percentages presented in Table 3, backfilled sites exhibit a more or less homogeneous distribution with a dominant part of sand in all depths, which even shows a decreasing trend from the upper to the lower parts of the soil profiles. In the case of CUT EX, this actually leads to silt being the dominant grain size. This pattern is also observable in the box-plot diagrams (Figure 6), where undisturbed sites (FOR, CUT) show decreasing clay and silt content with increasing depth, while backfilled sites show the opposite trend (Figure 6, Table 4).

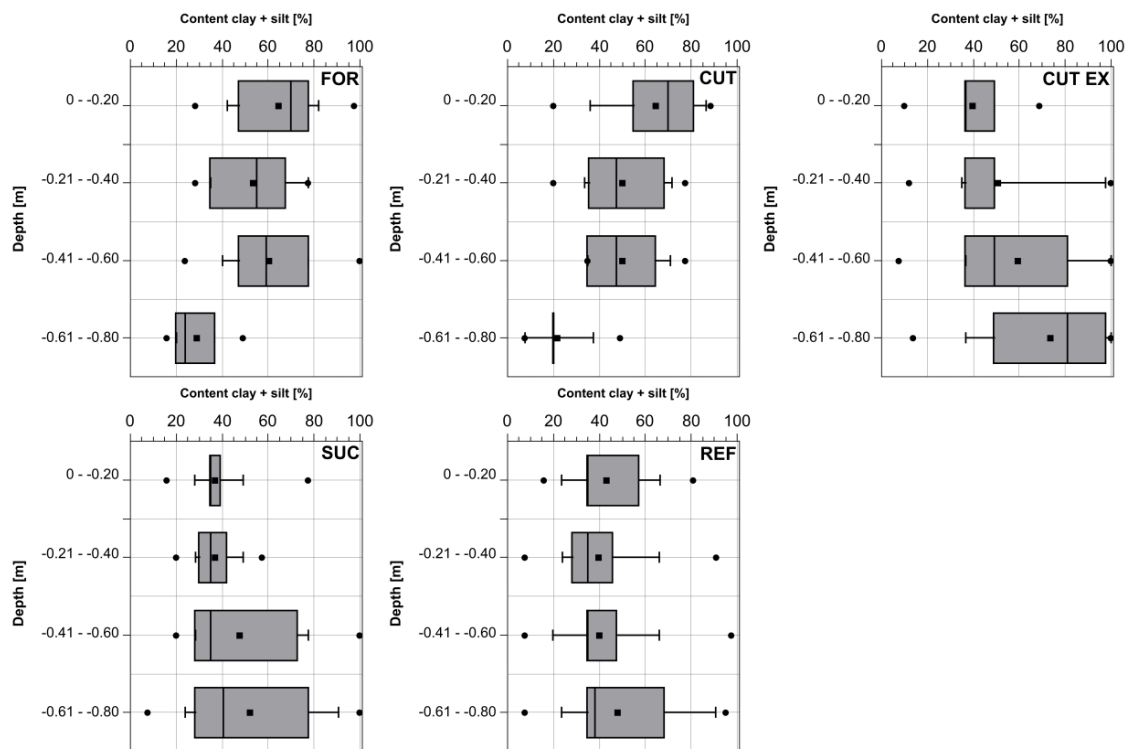


Figure 6. Clay and silt content dataset distribution.

Table 4. Mean content clay + silt. Depth aggregated data.

Depth [m]	Mean Content Clay + Silt [%]				
	FOR	CUT	CUT EX	SUC	REF
0--0.20	64.5	64.7	39.6	37.0	43.4
-0.21--0.40	53.6	50.1	50.6	37.0	39.8
-0.41--0.60	60.5	50.0	59.5	47.6	40.0
-0.61--0.80	29.0	22.0	73.4	52.3	48.0

Concerning soil moisture, there is also a noticeable difference between undisturbed and disturbed sites (Figure 7, Table 5).

Table 5. Mean soil moisture (SM). Depth aggregated data.

Depth [m]	Mean SM [%]				
	FOR	CUT	CUT EX	SUC	REF
0--0.20	31.7	43.0	30.5	27.1	28.0
-0.21--0.40	20.5	33.0	31.0	26.6	27.3
-0.41--0.60	21.6	33.4	28.8	25.1	27.1
-0.61--0.80	17.7	27.8	25.1	23.5	25.5

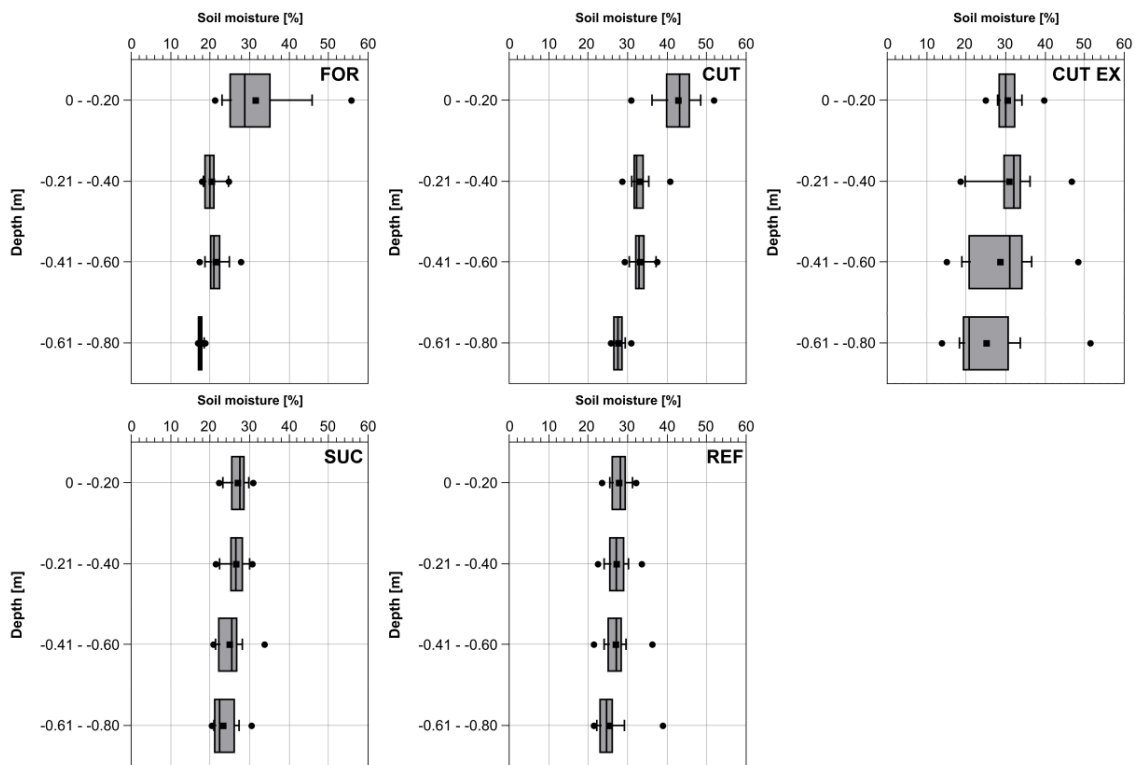


**Figure 7.** Soil moisture dataset distribution. Recorded in fall 2018 (FOR, CUT, SUC, REF) and early summer 2019 (CUT EX), carried out at the same time as penetrometer measurements.

Antecedent precipitation input is still preserved in undisturbed topsoil layers, as FOR and CUT clearly show increased soil moisture content in the upper parts of the soil profile. CUT throughout shows higher soil moisture values, most likely caused by the already cut-down forest stand, which eventually leads to less/no rainfall interception and/or water abstraction by trees. SUC and REF both show rather homogeneous depth profiles, indicating a faster water transport from top- to bottom-layers. This pattern is very likely linked to comparable SOM content patterns (Figure 8, Table 6), as SOM possesses good water binding properties. Both 2018 and 2019 datasets show comparable SM contents, therefore potentially exerting a similar influence on PR.

**Table 6.** Mean soil organic matter (SOM) content. Depth aggregated data.

Depth [m]	Mean SOM [%]				
	FOR	CUT	CUT EX	SUC	REF
0–0.20	16.0	19.4	8.1	7.7	7.6
–0.21–0.40	7.9	8.2	7.0	7.3	7.2
–0.41–0.60	8.6	8.4	6.2	5.5	7.0
–0.61–0.80	4.6	4.7	4.3	4.2	5.7

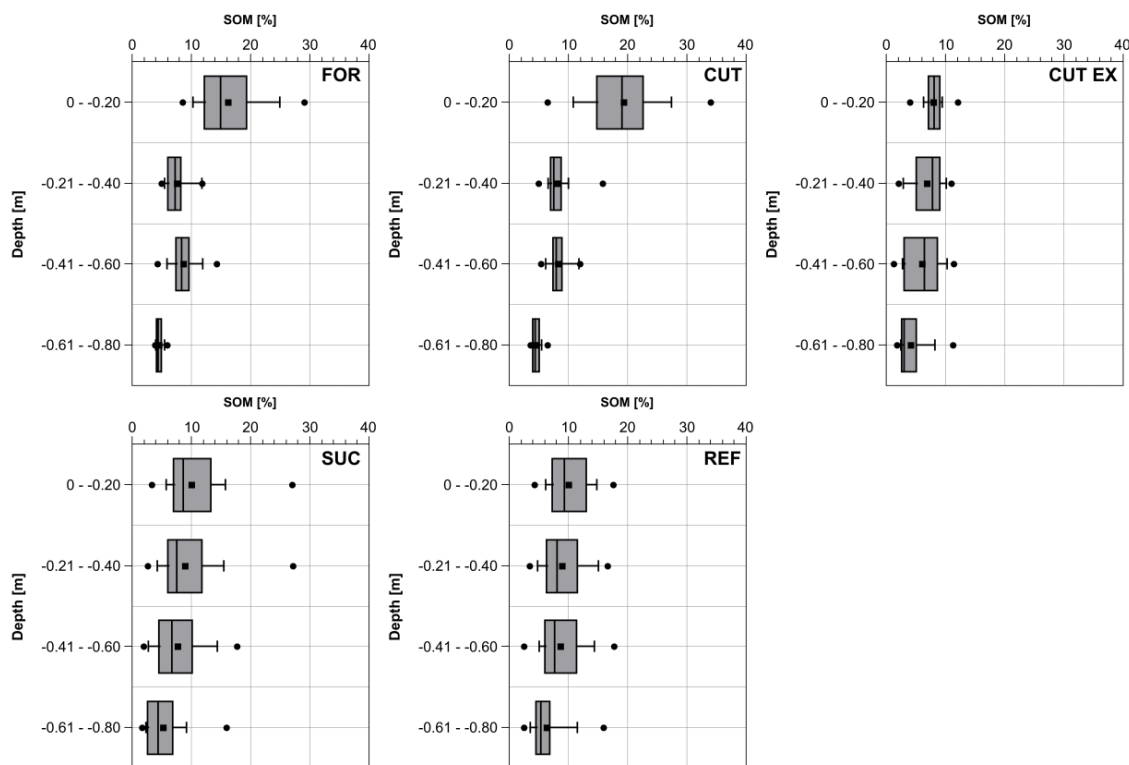


Figure 8. Soil organic matter (SOM) dataset distribution.

Concerning SOM, again, a clear difference between undisturbed and disturbed sites was found. While humic A-Horizons were/are existent on undisturbed sites—indicated by remarkably high SOM contents (SOM 16.0–19.4%) in the upper 0.2 m—a noteworthy drop of SOM-percentage is observable on disturbed sites. Here, the mean content is reduced more than 10% in the upper depth-class and it remains lower in all depth classes (Table 6). This is also a strong reference to proper backfilling practices: in the present case, thoroughly mixed material was backfilled. A separation of former topsoil during excavation and backfilling would lead to a less prominent loss of SOM and would also provide the opportunity to remodel a SOM-rich topsoil layer. Apart from that, the expectable SOM pattern with a distinctly higher SOM content in topsoil layers is only existent on undisturbed areas and all three disturbed areas show more or less homogeneous SOM distributions.

### 3.2. Penetration Resistance: Descriptive Analysis

Mean PR datasets are depicted in Figure 9 and Table 7, using depth-aggregated datasets.

Undisturbed soils (FOR, CUT) show comparable depth-patterns, which is also the case for old backfilled sites (SUC, REF); therefore, a clear distinction can be made (Figure 9): while undisturbed sites exhibit a continuously and constantly rising PR with depth, older disturbed sites show a distinct and sharp PR-increase in the upper 0.4 m, with PR increasing further in the two lower depth classes. CUT EX, the most recently backfilled site, is more comparable to undisturbed sites and additionally features rather low PR with increasing depth.

Even though there are PR max-values  $>2$  MPa, mean PR clearly stays  $<2$  MPa in the upper 0.2 m of all soil profiles, most likely indicating no noteworthy rooting restrictions (Table 7). Yet, viewing at  $-0.21$ – $-0.40$  m depth, older backfilled sites SUC and REF already show mean PR  $> 3$  MPa, while FOR, CUT and CUT EX stay below this threshold. FOR and CUT exceed 2 MPa within the next depth-class, while CUT EX still stays  $<2$  MPa, only exceeding it in the last depth-class, where all observed areas showed indications for affected root progression.

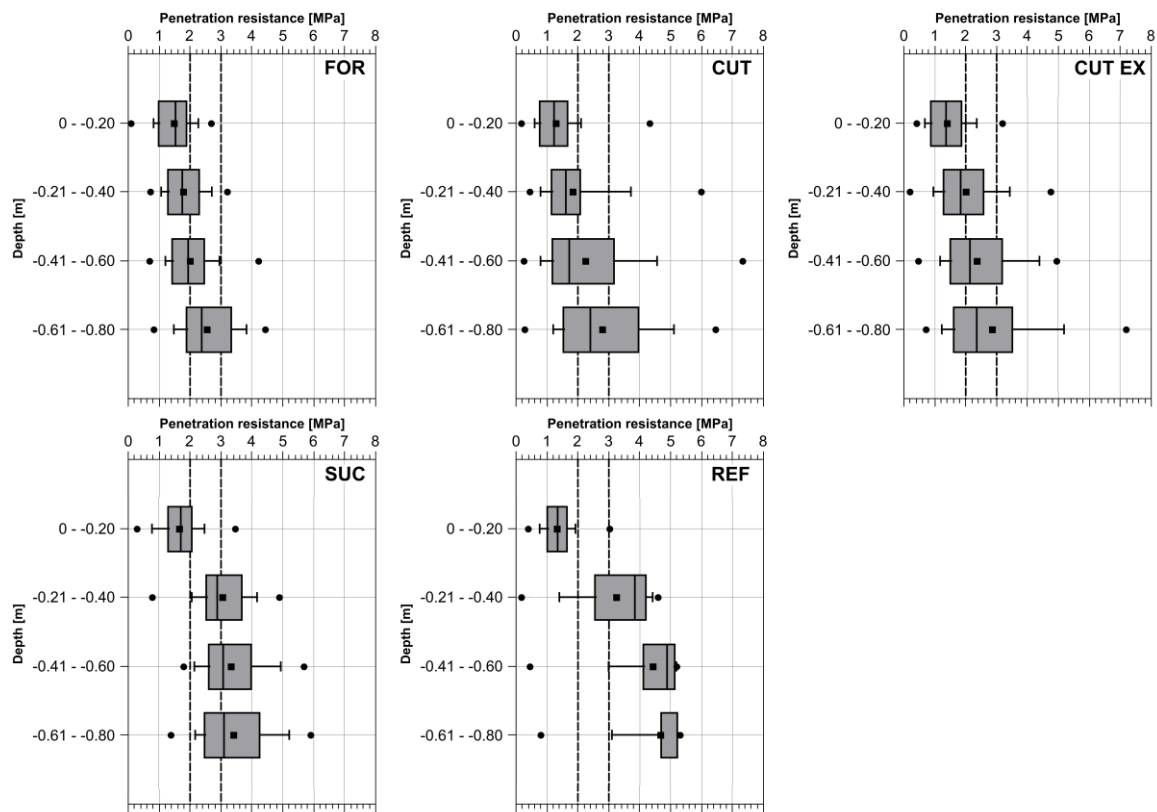


**Figure 9.** Penetration resistance (PR) dataset distribution. Dotted lines (2, 3 MPa) represent literature-based, critical PR affecting root growth according to [13].

**Table 7.** Descriptive statistics (mean, minimum, maximum, standard deviation ( $\sigma$ )) for penetration resistance (PR), depth aggregated data. Values >2 MPa indicated bold.

Depth [m]	PR [MPa]	FOR	CUT	CUT EX	SUC	REF
0--0.20	Mean	1.50	1.30	1.37	1.66	1.35
	Min	0.10	0.20	0.35	0.30	0.41
	Max	<b>2.71</b>	<b>4.33</b>	<b>3.21</b>	<b>3.47</b>	<b>3.03</b>
	$\sigma$	0.58	0.64	0.66	0.62	0.48
-0.21--0.40	Mean	1.81	1.86	1.72	<b>3.06</b>	<b>3.27</b>
	Min	0.73	0.47	0.49	0.80	0.20
	Max	<b>3.21</b>	<b>6.00</b>	<b>4.78</b>	<b>4.90</b>	<b>4.61</b>
	$\sigma$	0.61	1.12	0.80	1.71	1.59
-0.41--0.60	Mean	<b>2.01</b>	<b>2.27</b>	1.82	<b>3.35</b>	<b>4.44</b>
	Min	0.72	0.29	0.63	1.80	0.46
	Max	<b>4.25</b>	<b>7.34</b>	<b>4.78</b>	<b>5.70</b>	<b>5.21</b>
	$\sigma$	0.76	1.49	0.71	1.80	1.07
-0.61--0.80	Mean	<b>2.55</b>	<b>2.80</b>	<b>2.87</b>	<b>3.42</b>	<b>4.69</b>
	Min	0.84	0.30	0.70	1.4	0.80
	Max	<b>4.44</b>	<b>6.47</b>	<b>7.20</b>	<b>5.92</b>	<b>5.32</b>
	$\sigma$	0.98	1.55	1.80	1.89	0.98

### 3.3. Soil Characteristics and Penetration Resistance: Spatial Distribution

Spatial interpolations of clay and silt content (Figure 10) show a patchy pattern for all sites in the uppermost depth category with SUC exhibiting the lowest (C + Si) contents. Going deeper, a less patchy pattern is observable at FOR and CUT, indicating comparable and ubiquitous pedogenetic processes, which led to differentiated spatial patterns. For example, a band of higher (C + Si) content is visible at -0.21--0.40 m, retracing the slope geometry. At undisturbed sites, there is no distinctive

superior pattern observable but rather abrupt spatial changes, indicating thoroughly mixed, backfilled soil. Interpolation quality was found to be sufficient, as RMSE showed no noteworthy deviations (Table 8).

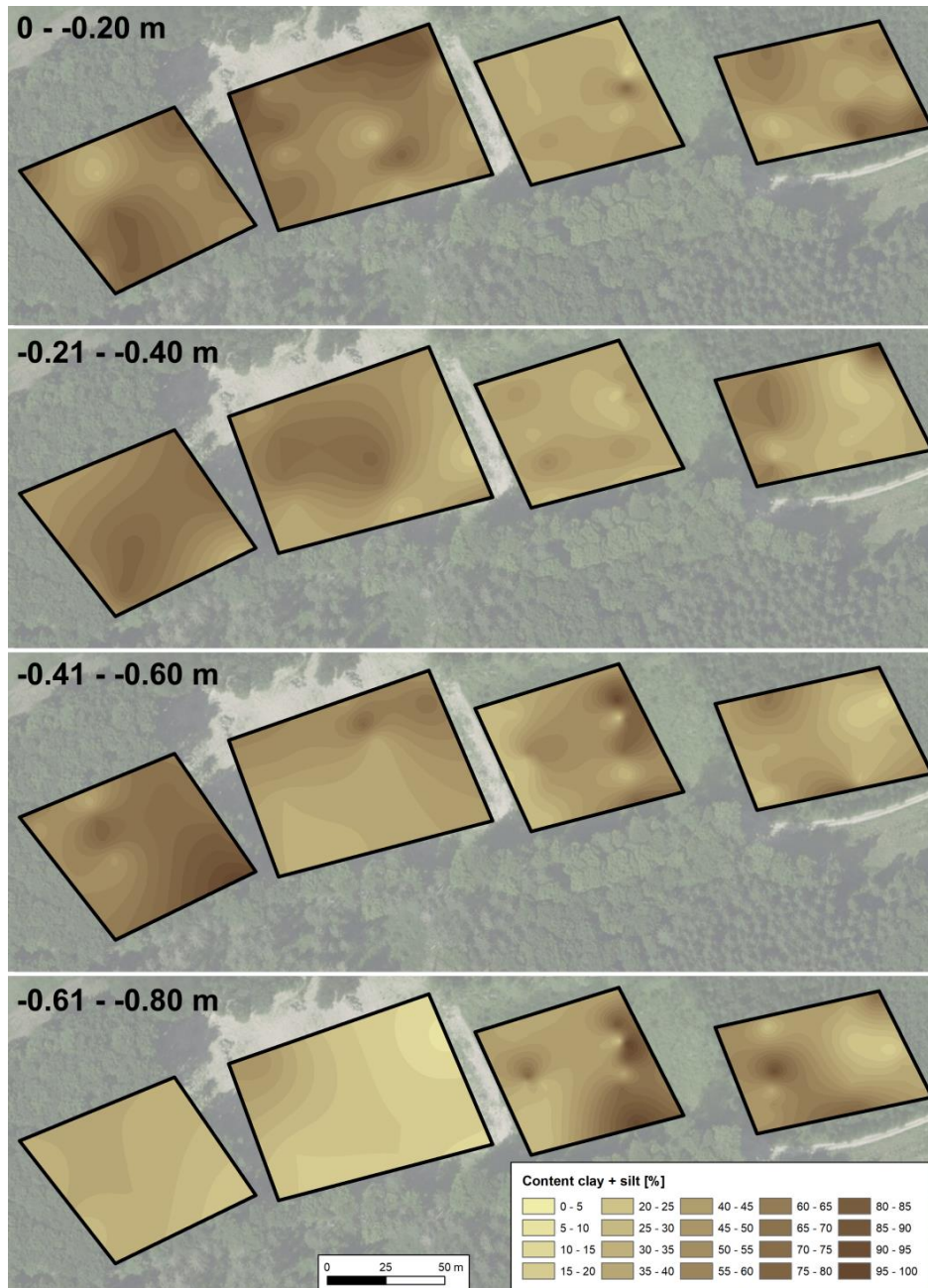


**Figure 10.** Interpolated content clay + silt. Aerial photography provided by LVermGeo RLP (2019).

Spatial SM datasets (Figure 11) clearly depict trends described in Section 3.1, with area CUT showing by far the highest soil water content. Overall, the highest SM values were found in the upper soil layer. Here, a spatial pattern is clearly visible, as highest values in both undisturbed sites are located at the foot of the slope, indicating a surface-near water movement that follows the main slope. On the backfilled sites, which have a smoother terrain, no comparable trend is visible. Totally undisturbed soil (FOR) shows a distinctive drop of SM in deeper zones, even beginning in depth

category  $-0.21$ – $-0.40$  m, this tendency is less prominent on disturbed sites. The RMSE for all raster datasets was satisfying (Table 9).

**Table 8.** Root mean square error (RMSE) interpolated raster clay + silt.

Depth [m]	RMSE Clay + Silt			
	FOR	CUT	SUC	REF
0– $-0.20$	$4.9 \times 10^{-8}$	$6.3 \times 10^{-8}$	$1.5 \times 10^{-8}$	$3.0 \times 10^{-8}$
$-0.21$ – $-0.40$	$1.1 \times 10^{-8}$	$1.8 \times 10^{-8}$	$1.4 \times 10^{-8}$	$2.5 \times 10^{-8}$
$-0.41$ – $-0.60$	$2.9 \times 10^{-8}$	$3.0 \times 10^{-8}$	$4.1 \times 10^{-8}$	$1.4 \times 10^{-8}$
$-0.61$ – $-0.80$	$4.3 \times 10^{-9}$	$1.2 \times 10^{-8}$	$3.8 \times 10^{-8}$	$2.8 \times 10^{-8}$

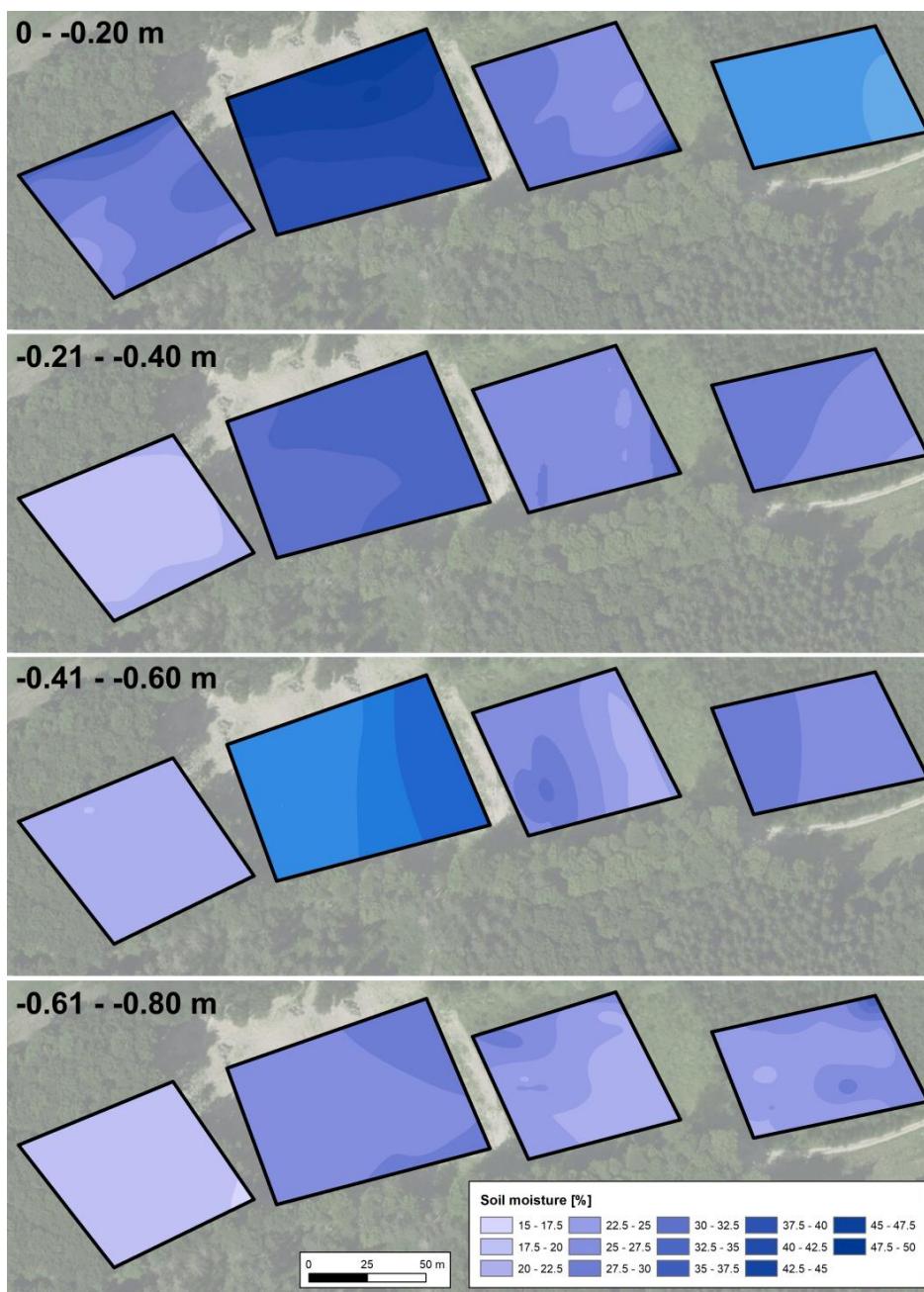


**Figure 11.** Interpolated soil moisture. Aerial photography provided by LVerMGeo RLP (2019).

Analogous to soil moisture datasets, interpolated soil organic matter data generally retraces findings explained in Section 3.1, as the highest contents are located in the upper soil layer of undisturbed sites, which is an expectable pattern for forest soils. Yet, singular areas on CUT show comparably high SOM content, even exceeding 30%, and therefore indicating organic soil horizons (Figure 12). This might be caused by accumulation of eroded topsoil, as these areas are situated at the foot of the slope and CUT was already deforested, leaving topsoil prone to water erosion. Several heavy rainfall events that occurred in late summer could have triggered erosion processes; yet, no distinct channeling was observable, therefore sheet erosion would be the most likely accountable process. Disturbed sites show constantly lower SOM content, indicating the removal of former organic and/or humic A-Horizons and thoroughly mixed, backfilled soil material. Again, RMSE shows satisfactory results (Table 10).

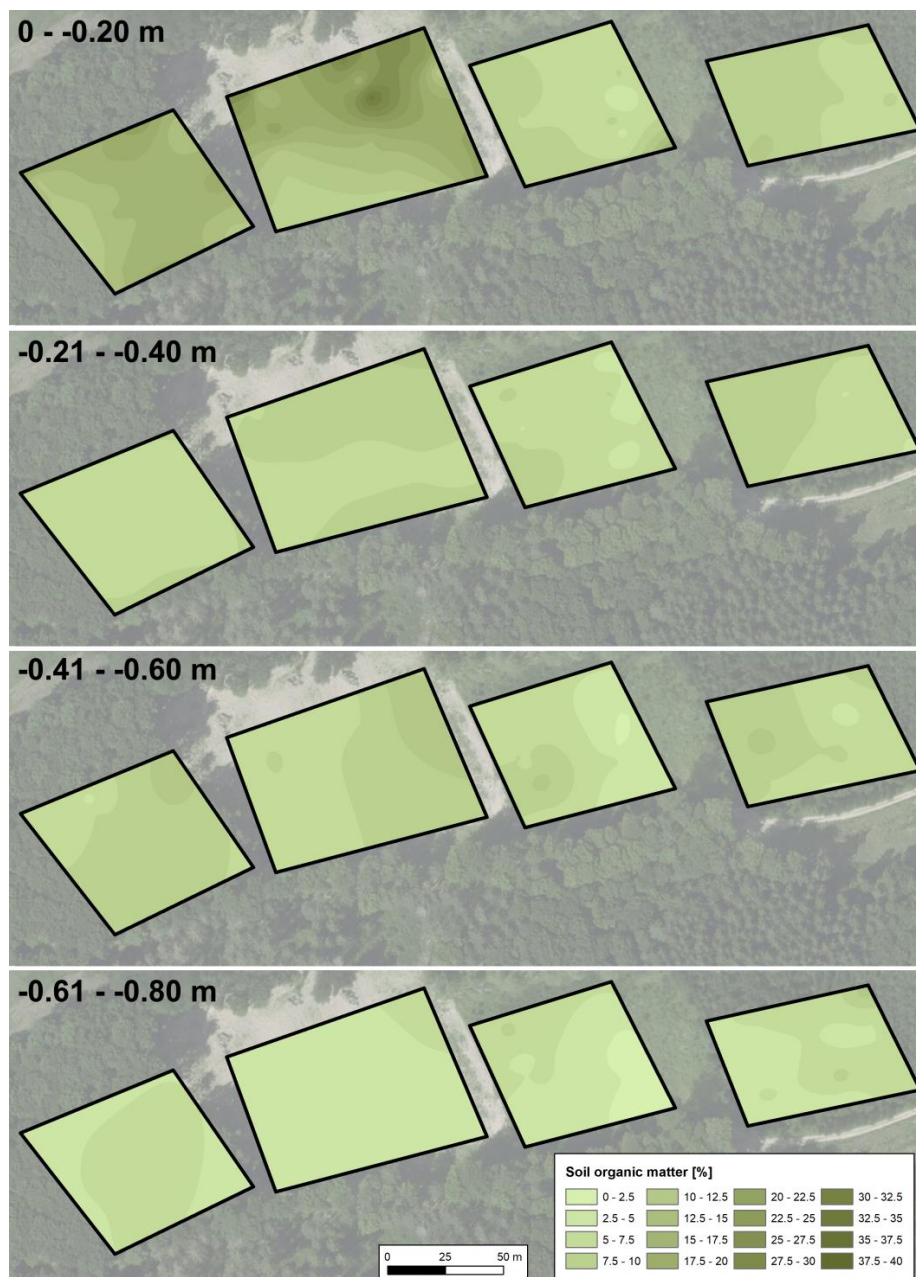


**Figure 12.** Interpolated soil organic matter, depth 0–0.20 m. Aerial photography provided by LVerMGeo RLP (2019).

**Table 9.** Root mean square error (RMSE) interpolated raster soil moisture.

RMSE Soil Moisture				
Depth [m]	FOR	CUT	SUC	REF
0--0.20	$2.1 \times 10^{-8}$	$2.1 \times 10^{-8}$	$2.9 \times 10^{-8}$	$2.6 \times 10^{-8}$
-0.21--0.40	$1.6 \times 10^{-8}$	$3.6 \times 10^{-8}$	$2.4 \times 10^{-8}$	$1.7 \times 10^{-8}$
-0.41--0.60	$2.0 \times 10^{-8}$	$4.1 \times 10^{-11}$	$1.4 \times 10^{-8}$	$2.2 \times 10^{-8}$
-0.61--0.80	$5.1 \times 10^{-9}$	$8.0 \times 10^{-12}$	$1.7 \times 10^{-8}$	$5.8 \times 10^{-9}$

**Table 10.** Root mean square error (RMSE), interpolated raster soil organic matter.

RMSE Soil Organic Matter				
Depth [m]	FOR	CUT	SUC	REF
0--0.20	$1.1 \times 10^{-8}$	$1.0 \times 10^{-8}$	$1.0 \times 10^{-8}$	$2.4 \times 10^{-9}$
-0.21--0.40	$9.1 \times 10^{-9}$	$8.4 \times 10^{-9}$	$6.5 \times 10^{-9}$	$7.2 \times 10^{-9}$
-0.41--0.60	$6.4 \times 10^{-9}$	$2.3 \times 10^{-10}$	$2.8 \times 10^{-9}$	$4.2 \times 10^{-9}$
-0.61--0.80	$1.2 \times 10^{-9}$	$2.5 \times 10^{-12}$	$4.3 \times 10^{-9}$	$2.0 \times 10^{-9}$

Spatial patterns of soil characteristics on CUT EX (Figure 13) show indications for certain backfilling actions: Beginning in the second depth class, increased clay and silt content is visible at the east/northeast half of the area. Here, soil moisture and soil organic matter content is in contrast relatively decreased. Low SOM and high C + Si are most likely an indicator for backfilled former subsoil material, originating from weathered B-Horizons. The RMSE of all datasets was again satisfying (Table 11).

**Table 11.** Root mean square error (RMSE), interpolated raster datasets of CUT EX.

RMSE Area CUT EX			
Depth [m]	Clay + Silt	Soil Moisture	Soil Organic Matter
0--0.20	$7.1 \times 10^{-9}$	$1.4 \times 10^{-8}$	$3.9 \times 10^{-8}$
-0.21--0.40	$8.0 \times 10^{-9}$	$2.2 \times 10^{-8}$	$3.4 \times 10^{-8}$
-0.41--0.60	$2.7 \times 10^{-9}$	$2.1 \times 10^{-8}$	$1.9 \times 10^{-8}$
-0.61--0.80	$1.7 \times 10^{-9}$	$2.2 \times 10^{-8}$	$3.9 \times 10^{-8}$

Interpolated PR datasets show more or less distinct spatial patterns (Figure 14). Most strikingly, a consistent zone of high PR exists in the SE corner of CUT, starting at -0.21--0.40 m and expanding in deeper soil layers. This proves that natural heterogeneities of possible rooting restrictions (indicated red/purple) exist on undisturbed sites. On FOR, area-wide rooting restrictions begin to form at -0.41 m and deeper. Yet, there are still subareas that show PR < 2 MPa (indicated blue) even at -0.61--0.80 m on undisturbed sites. The distinct PR-shift on disturbed sites already described in Section 3.2 and beginning with the second soil layer, is clearly visible. From -0.21 m on, there are solely values >2 MPa. The RMSE proved to be sufficient (Table 12). Because of the larger number and denser spatial distribution of singular input data points, the PR RMSE is higher than those of general soil characteristics (Tables 8–11).

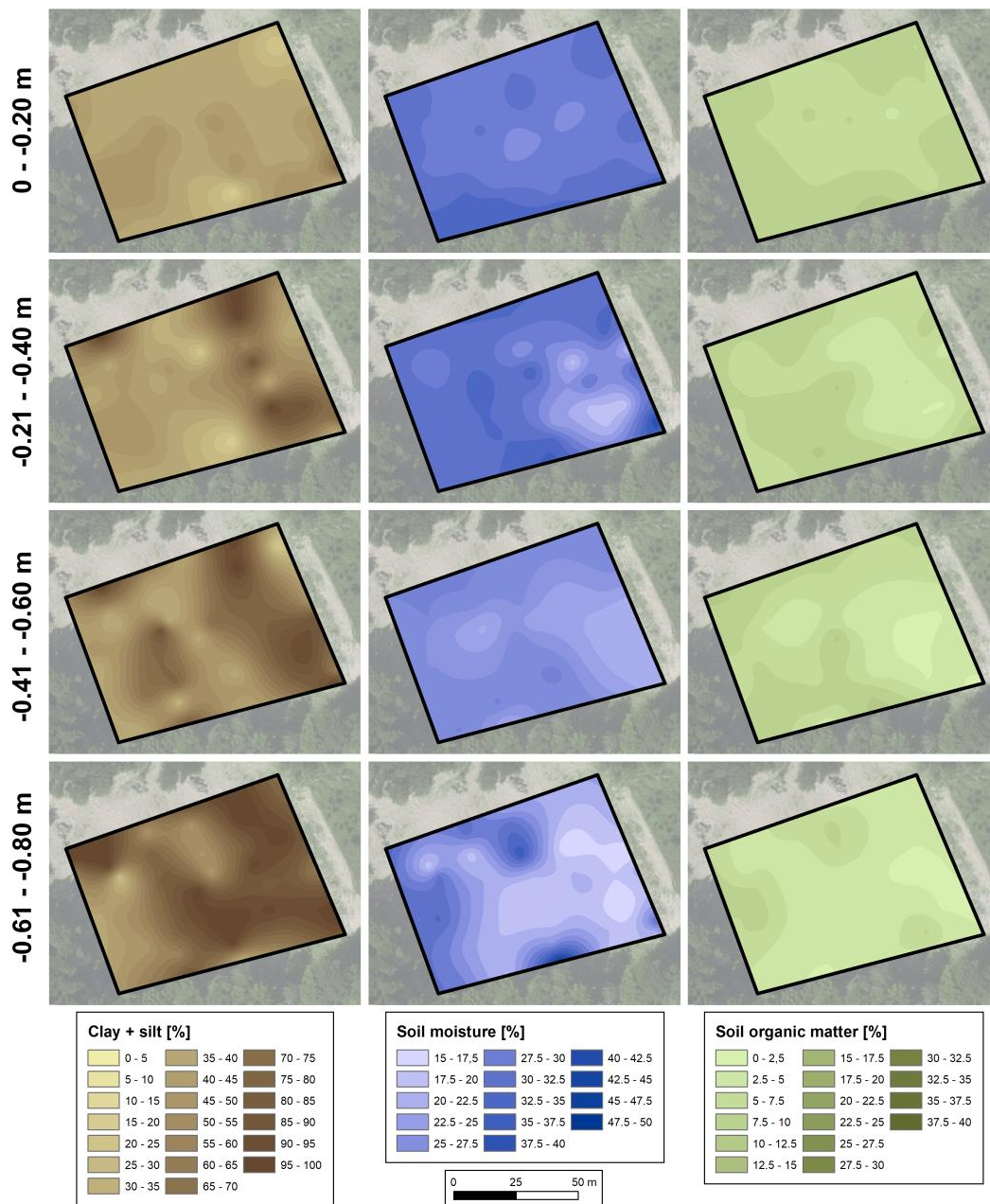


Figure 13. Interpolated soil characteristics, CUT EX. Aerial photography provided by LVermeGeo RLP (2019).

Table 12. Root mean square error (RMSE), interpolated raster datasets (penetration resistance).

Depth [m]	RMSE Penetration Resistance			
	FOR	CUT	SUC	REF
0--0.20	0.17	0.19	0.35	0.22
-0.21--0.40	0.19	0.25	0.34	0.33
-0.41--0.60	0.24	0.34	0.34	0.20
-0.61--0.80	0.33	0.41	0.32	0.20

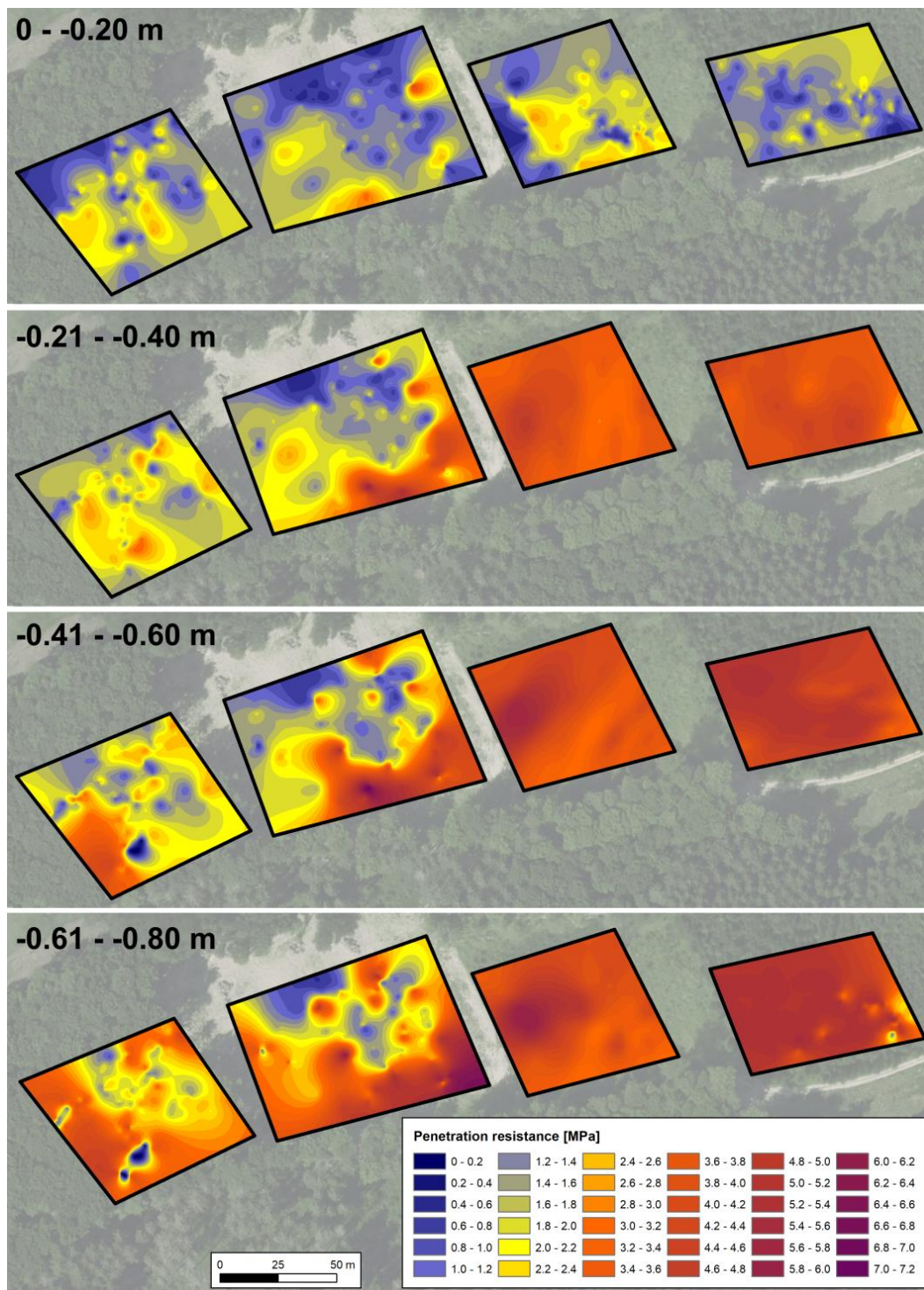
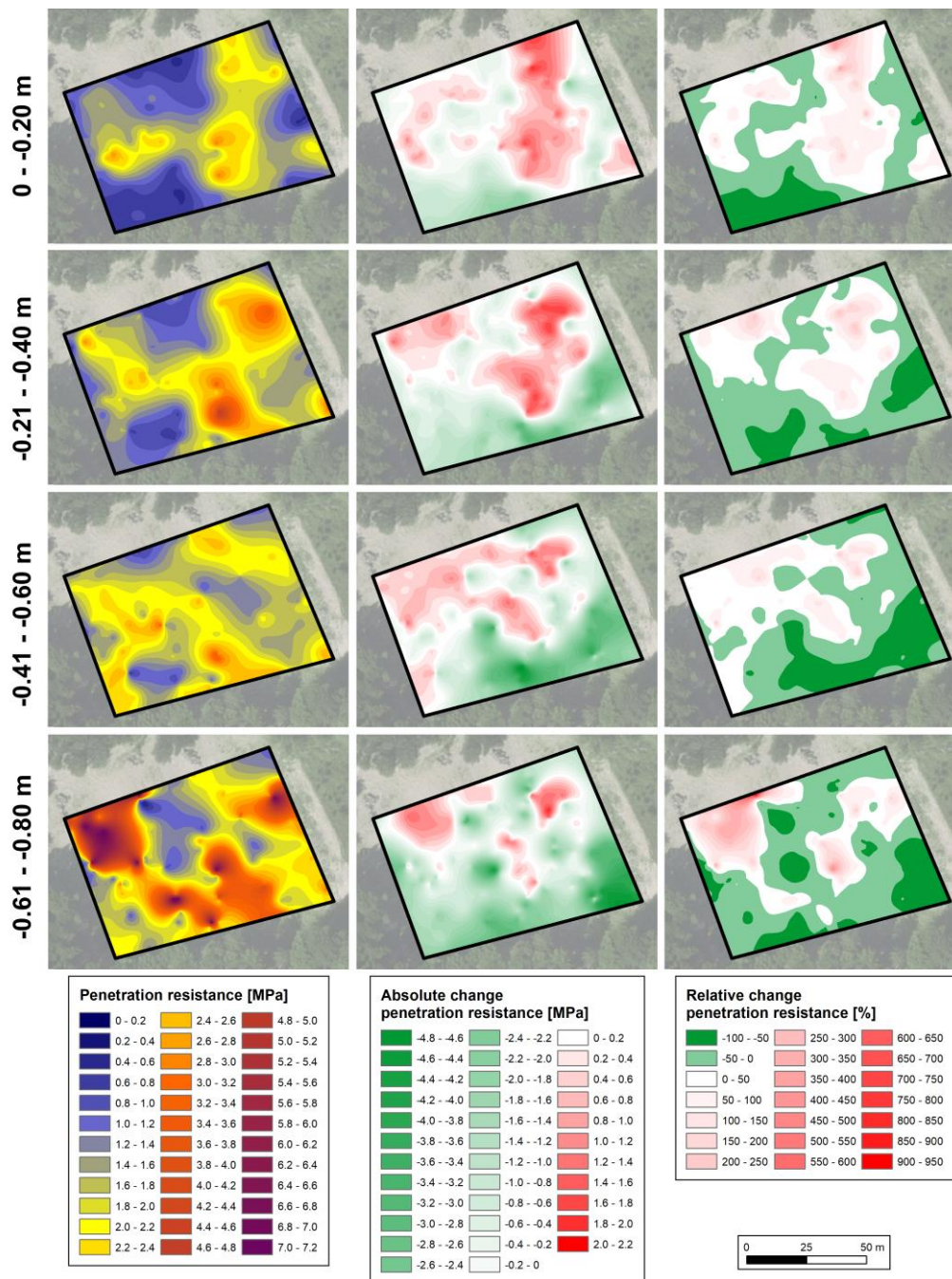


Figure 14. Interpolated penetration resistance. Aerial photography provided by LVerMGeo RLP (2019).

Figure 15 shows the PR of CUT EX. As this area provided the possibility to compare before/after excavation states, absolute and relative deviation of the PR from CUT is also depicted.



**Figure 15.** Interpolated penetration resistance, absolute and relative change of penetration resistance, CUT EX compared to CUT. Aerial photography provided by LVerGeo RLP (2019).

CUT EX shows two prominent corridors of increased PR, both starting in the SE corner and continuing to the NE and NW respectively. The SE–NW corridor shows by far the highest PR, located in the very bottom soil layer. Yet, there are still parts of CUT EX that show PR < 2 MPa even at –0.61––0.80 m. Changes in PR are distinct areas that formerly featured low PR (NW corner) and now show high PR and vice versa (SE corner). Therefore, absolute changes between –4.77 and 6.49 MPa and relative changes between –79% and 906% are observable. However, looking at mean changes, a minimal reduction of absolute PR is observable, with topsoil being the only exception (Figure 16, Table 13).

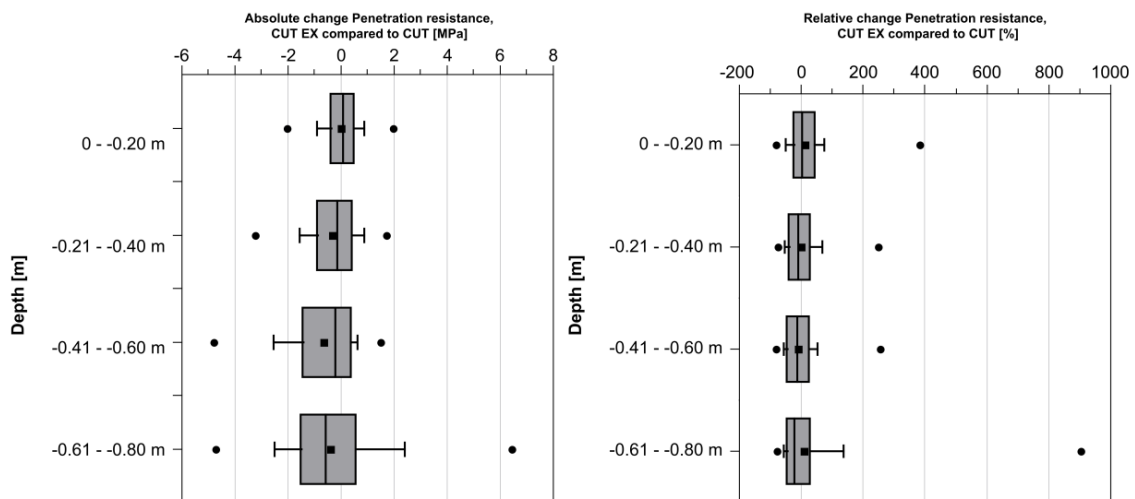


Figure 16. Absolute and relative change of penetration resistance, CUT EX compared to CUT.

Table 13. Descriptive statistics for absolute and relative change of penetration resistance (PR), depth aggregated data. Area CUT EX compared to area CUT.

Depth [m]		Absolute Change PR [MPa]	Relative Change PR [%]
0--0.20	Mean	0.03	13.9
	Min	-2.01	-78.6
	Max	2.00	387
-0.21--0.40	Mean	-0.27	1.38
	Min	-3.19	-71.3
	Max	1.8	253.2
-0.41--0.60	Mean	-0.61	-6.4
	Min	-4.77	-79.0
	Max	1.54	257.1
-0.61--0.80	Mean	-0.37	12.2
	Min	-4.69	-76.1
	Max	6.49	906.0

### 3.4. Statistical Comparison of Undisturbed and Disturbed Sites

Further on, a statistical comparison of undisturbed and disturbed sites was carried out. An initial Kolmogorov–Smirnov test showed mixed results, as only six datasets were normally distributed (Table 14).

Table 14. Results of the Kolmogorov–Smirnov test for depth aggregated data. Normally distributed datasets ( $p > 0.05$ ) are indicated bold.

Depth [m]		FOR	CUT	CUT EX	SUC	REF
0--0.20	n	150	150	153	150	150
	p	<b>0.200</b>	<b>0.200</b>	0.000	<b>0.200</b>	<b>0.200</b>
-0.21--0.40	n	150	150	153	120	68
	p	0.033	0.000	0.002	0.004	0.003
-0.41--0.60	n	147	150	150	106	34
	p	0.012	0.000	0.002	<b>0.121</b>	0.001
-0.61--0.80	n	144	149	137	101	29
	p	0.003	0.000	0.000	<b>0.200</b>	0.050

As the majority of the observed data was not normally distributed, the Kruskal–Wallis test was chosen to determine statistical similarities (Table 15).

**Table 15.** Kruskal–Wallis test for all areas (FOR, CUT, CUT EX, SUC, REF). Significantly different areas ( $p < 0.05$ ) are indicated bold.

Depth [m]	$p$
0–0.20	<b>0.000</b>
–0.21–0.40	<b>0.000</b>
–0.41–0.60	<b>0.000</b>
–0.61–0.80	<b>0.000</b>

The simplified test, only comparing all sub-areas within one analysis, shows  $p = 0.000$  for all depths, indicating significantly dissimilar ( $p < 0.05$ ) datasets. In order to obtain a more detailed analysis, a pairwise Kruskal–Wallis test was carried out for every sub-area and depth (Table 16).

**Table 16.** Pairwise Kruskal–Wallis test. Significantly different areas ( $p < 0.05$ ) are indicated bold.

Depth [m]		FOR	CUT	CUT EX	SUC
0–0.20	CUT	<b>0.010</b>	–	–	–
	CUT EX	1.000	0.515	–	–
	SUC	0.233	<b>0.000</b>	<b>0.020</b>	–
	REF	0.204	1.000	1.000	<b>0.000</b>
–0.21–0.40	CUT	1.000	–	–	–
	CUT EX	1.000	1.000	–	–
	SUC	<b>0.000</b>	<b>0.000</b>	<b>0.000</b>	–
	REF	<b>0.000</b>	<b>0.000</b>	<b>0.000</b>	1.000
–0.41–0.60	CUT	1.000	–	–	–
	CUT EX	1.000	0.426	–	–
	SUC	<b>0.000</b>	<b>0.000</b>	<b>0.000</b>	–
	REF	<b>0.000</b>	<b>0.000</b>	<b>0.000</b>	1.000
–0.61–0.80	CUT	1.000	–	–	–
	CUT EX	<b>0.000</b>	0.156	–	–
	SUC	<b>0.000</b>	<b>0.000</b>	<b>0.000</b>	–
	REF	<b>0.000</b>	<b>0.000</b>	<b>0.000</b>	1.000

With only one exception, namely the topsoil layer, undisturbed sites (FOR, CUT) show statistically similar results. This is rather expectable, considering the generally more heterogeneous dataset distribution in this depth. Apart from that, both REF and SUC exhibit mostly similar penetration resistances, showing a consistent similarity with increasing depth. Recently backfilled soil at CUT EX is often comparable to undisturbed soil, but there are observable deviations indicating altered PR, especially in deeper soil zones (cf. Sections 3.2 and 3.3).

Concluding, a simplified approach was used, comparing undisturbed with disturbed sites: Both FOR and CUT were aggregated to the new category “Undisturbed”, as the Kruskal–Wallis test showed overall statistically similar datasets. On the basis of this established benchmark-category, deviations from an undisturbed state could be calculated (Figure 17).

It is clear to see, that the youngest backfilled site (CUT EX)—while still showing areas with increased PR (cf. Section 3.3)—is the only site with mainly reduced PR, contrasting with the older areas SUC and REF, which show notable PR increases. The general exception is the topsoil layer, where all areas show only small deviations.

Again, simplified and pairwise Kruskal–Wallis tests were performed, testing backfilled areas and the combined, undisturbed dataset regarding their similarities. As expected, the simplified Kruskal–Wallis tests showed overall significantly differing datasets, except for the topsoil layer (Table 17).

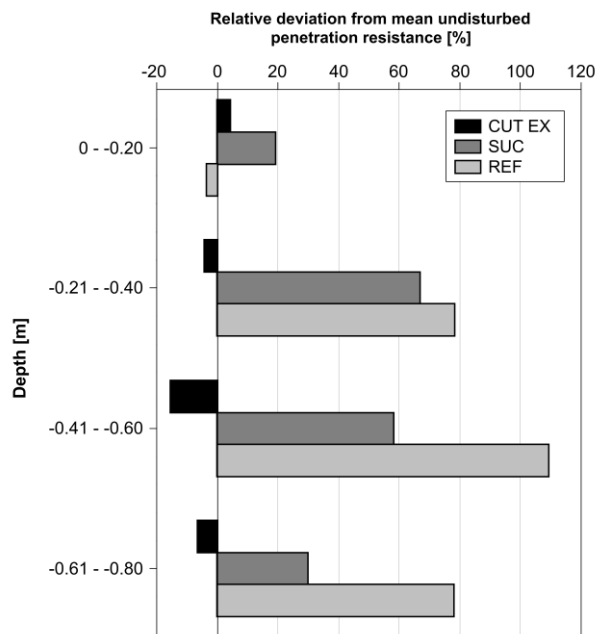


**Figure 17.** Relative penetration resistance deviation of backfilled areas compared to undisturbed soil; depth-aggregated data.

**Table 17.** Kruskal–Wallis test for simplified areas (Undisturbed, CUT EX, SUC, REF). Significantly different areas ( $p < 0.05$ ) are indicated bold.

Depth [m]	<i>p</i>
0–0.20	0.067
–0.21–0.40	<b>0.000</b>
–0.41–0.60	<b>0.000</b>
–0.61–0.80	<b>0.000</b>

The pairwise Kruskal–Wallis test revealed that CUT EX features a statistically similar dataset compared to undisturbed conditions, while SUC and REF consistently show dissimilar datasets, except topsoil on REF, which showed only minimal deviations from the undisturbed state (cf. Table 18).

**Table 18.** Pairwise Kruskal–Wallis test, comparing disturbed and aggregated undisturbed areas. Significantly different areas ( $p < 0.05$ ) are indicated bold.

Depth [m]		CUT EX	SUC	REF
0–0.20	Undisturbed	1.000	<b>0.000</b>	1.000
–0.21–0.40	Undisturbed	1.000	<b>0.000</b>	<b>0.000</b>
–0.41–0.60	Undisturbed	0.182	<b>0.000</b>	<b>0.000</b>
–0.61–0.80	Undisturbed	0.092	<b>0.000</b>	<b>0.000</b>

### 3.5. Correlation Analysis and ANOVA

Concluding correlation analysis and ANOVA showed ambiguous results. Spearman-correlations for PR and its supposedly governing factors show a consistent trend for SM, SOM and depth (Table 19).

**Table 19.** Spearman-correlation for penetration resistance (PR), clay + silt content (C + Si), soil moisture (SM), soil organic matter (SOM). Strong ( $< -0.700$ ,  $> 0.700$ ) and very strong ( $< -0.900$ ,  $> 0.900$ ) correlations are indicated bold.

	PR FOR (n = 600)	PR CUT (n = 600)	PR CUT EX (n = 612)	PR SUC (n = 600)	PR REF (n = 600)
C + Si	-0.18 **	-0.51 **	0.33 **	0.14 **	-0.06 **
SM	-0.36 **	-0.40 **	-0.30 **	-0.28 **	-0.35 **
SOM	-0.35 **	-0.39 **	-0.32 **	-0.28 **	-0.36 **
Depth	0.41 **	0.40 **	0.29 **	0.54 **	<b>0.79 **</b>

\*\* significant correlation ( $p < 0.01$ ).

SM and SOM show negative correlations, while depth is correlated positively. While all correlations are significant, only weak and moderate correlations were found except depth on REF. In the case of (C + Si), there is not even a consistent trend, as there are both negative and positive correlations.

Concluding, an ANOVA was carried out to determine multi-factorial dependencies between PR and its most likely governing factors. Class breaks, basing on predefined quantiles (cf. Section 2) are shown in Table 20.

**Table 20.** Class breaks for dependent factors (Content clay + silt (C + Si), soil moisture (SM), soil organic matter (SOM)), based on quantiles.

Quantile	Class	Class Break Value [%]		
		(C + Si)	SM	SOM
10%	1	30.8	19.6	3.9
25%	2	36.8	23.0	5.2
50%	3	46.5	26.7	6.8
75%	4	61.1	30.6	8.4
90%	5	72.1	33.7	12.2

Figure 18 shows relative shares of (C + Si)-, SM- and SOM-classes for each area and depth. Viewing at rather stable parameters ((C + Si) and SOM), undisturbed soils tend to show less wide dataset distributions per depth, indicating evolved pedogenetic horizons with rather constant and characteristic properties over all sampling points. On the other hand, backfilled sites show more fragmented class distributions.

Resulting significant factors, calculated via ANOVA, are listed in Table 21. Overall, no medium (0.25 or higher) or large (0.40 or higher) effect sizes were identified.

**Table 21.** Sorted effect sizes (f) of all significant ( $p < 0.05$ ) factors affecting penetration resistance.

Factor(s)	f
Depth	0.167
(C + Si) × Area	0.136
Depth × (C + Si) × Area	0.097
Area	0.095
SOM × Area	0.088

The largest effect size was achieved for depth, representing rising PR with increasing depth. The second largest effect size was calculated for the combined factor of (C + Si) and area. The remaining three significant factors show comparable, smaller effect sizes and involve factor "Area", or "Area" in combination with Depth, (C + Si) or SOM.

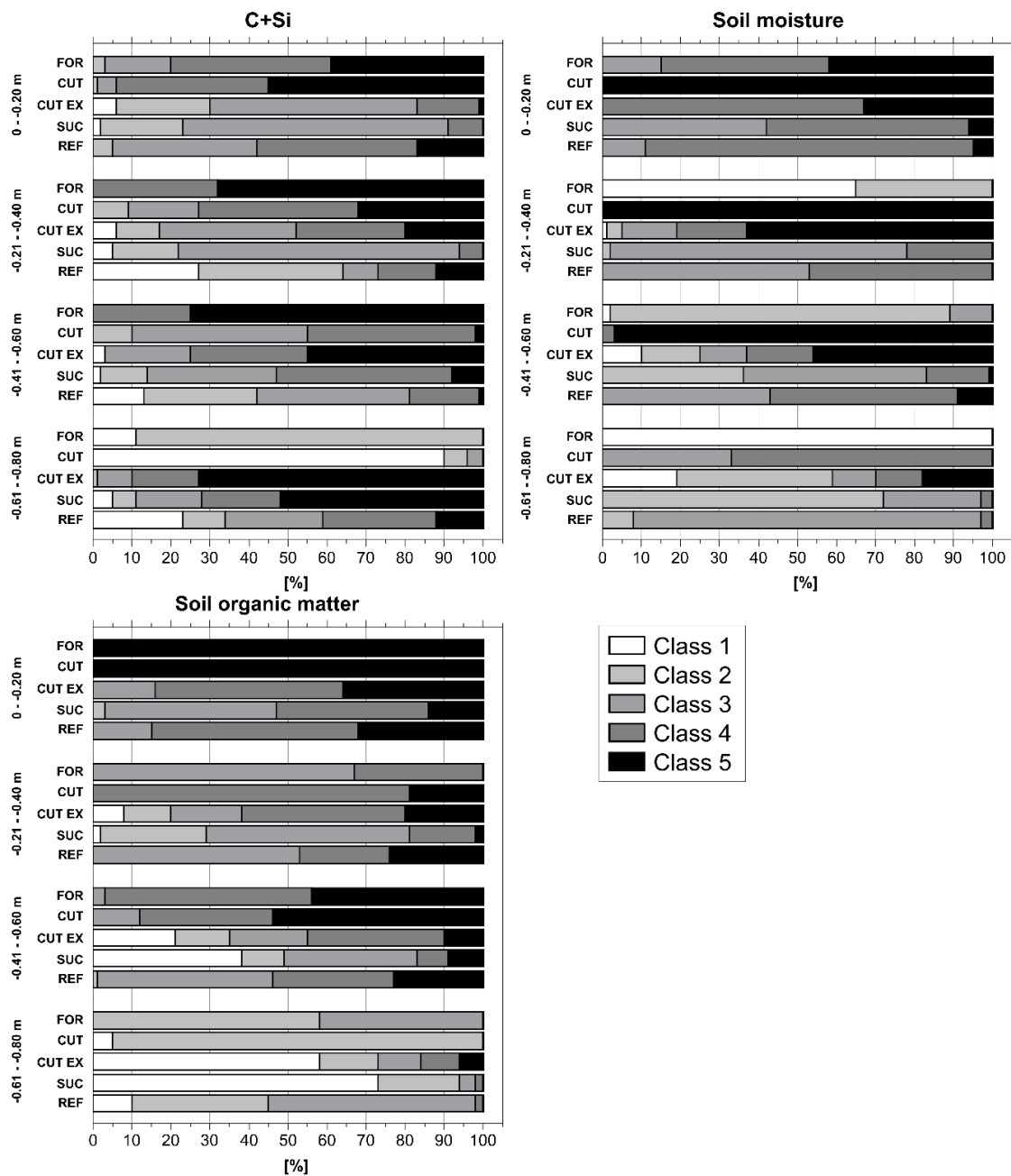


Figure 18. Relative shares of factor-classes used for ANOVA.

#### 4. Discussion

It is difficult to universally classify the PR results found in this study. The two main reasons—besides the fact that there are no consistent datasets for Andosols apart from this study—are: (a) differing literature values for PRs that affect root growth and elongation, and (b) the underlying consideration, what kind of vegetation is the subject of the analysis. The latter is often the reason for differing literature values for critical PR. Fundamentally, the most consistent range of critical PR lies between 1.8 and 2.0 MPa, with [53] reporting the lowest values (rooting affected > 1.4 MPa and restricted > 1.8 MPa) and other studies stating 2.0 MPa as a critical threshold value [2,13]. Viewing at the mean PR values, undisturbed LST-Andosols exhibit noticeably low PRs, especially in the upper 0.4 m, compared to other forest soils [54].

With *Fagus sylvatica* forests being the potential natural vegetation in the investigation area [55,56] and given the fact that *Fagus sylvatica* is/was the main tree species planted on FOR, CUT and CUT

EX, this seems to be a promising result, as studies point out, that root systems of *Fagus sylvatica* show highest densities in the upper 0.2–0.5 m [57,58]. Yet, a noteworthy number of roots was reported in depths up to 1.5 m in sandy soils [58], that is why not only the topmost soil layer has to be considered when classifying the results.

Overall, Ref. [13] most likely provides the best benchmark values for root growth, as this study was conducted at forested and sandy, backfilled sites just like the ones observed in this study. Yet, one has to consider that pumice particles may provide lower PR due to their low specific particle density. Besides that, Ref. [13] broke PR down into three major classes, <2 MPa, 2–3 MPa and >3 MPa, representing low, medium and high root growth restriction. This gave the possibility to visualize the datasets on the basis of an established categorization (Figures 19 and 20).

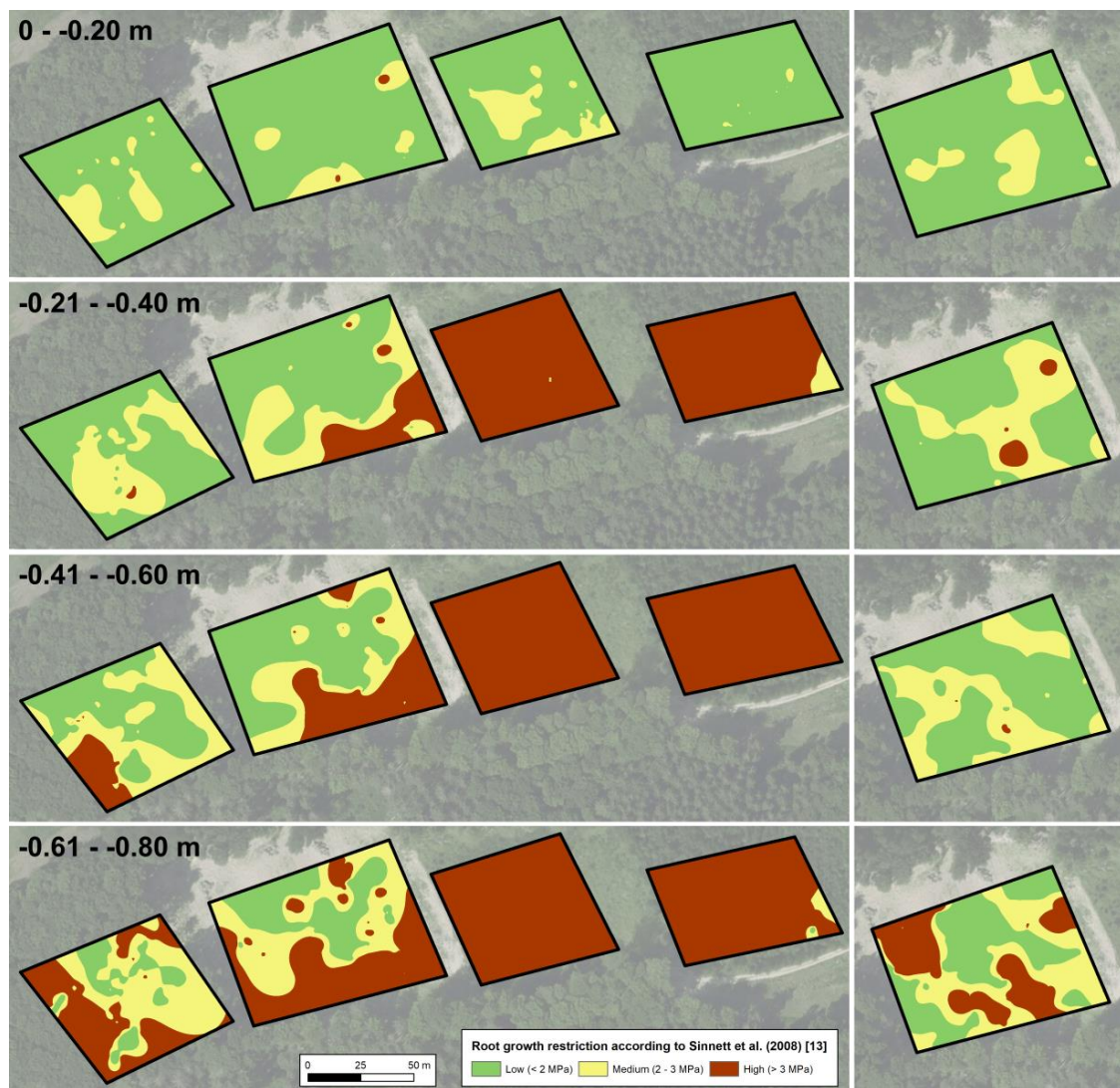


**Figure 19.** Interpolated penetration resistance, root growth restriction classes according to [13]. Right column: Area CUT EX.

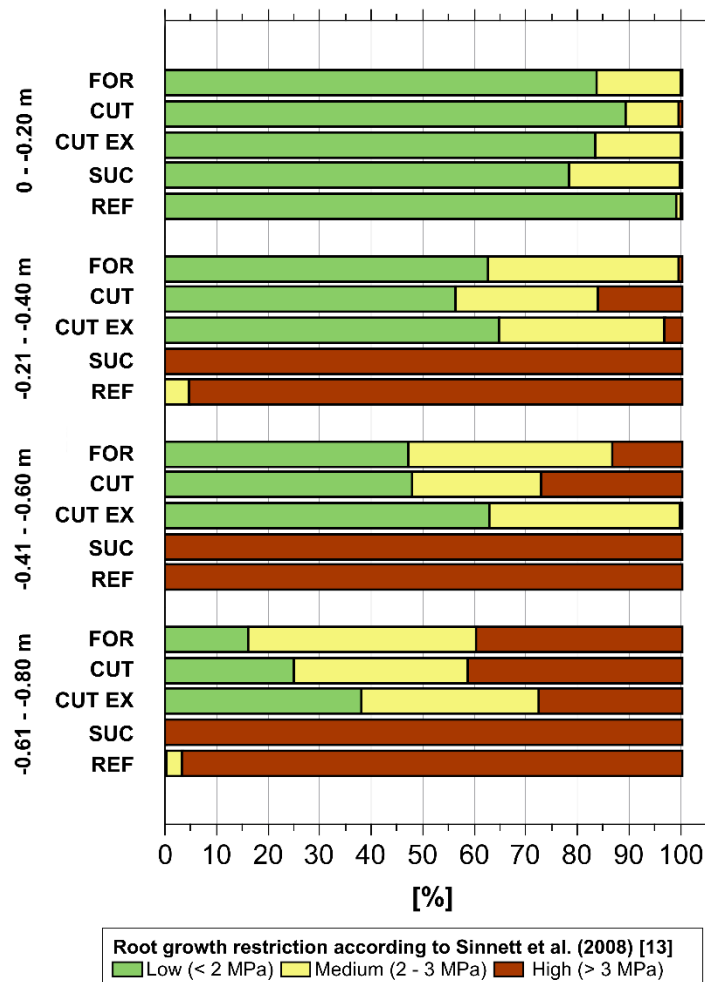


**Figure 20.** Relative shares of root growth restriction classes according to [13], interpolated datasets.

Using these categories, it is clear to see, that backfilled sites show PRs that most likely will affect root growth and elongation. Critical values even begin at  $-0.21$  m and show, almost exclusively,  $PR > 3$  MPa. The only exception is CUT EX, which was recently backfilled. Here, particularly low PR was found. These findings were also supported by the statistical comparison between undisturbed and disturbed sites, which showed the most satisfying and clear results within the whole statistical analysis.

Here, especially the pairwise Kruskal–Wallis test showed similarities between both undisturbed sites and between disturbed sites, with only CUT EX representing a disturbed site that is more comparable to undisturbed conditions. A possible explanation for this is that the backfilled soil at CUT EX has not consolidated yet, as backfilling took place only a few months before PR measurements. Useful studies concerned with self-weight soil consolidation are scarce, as the majority of consolidation analysis has studied construction sites and their soil stability or self-weight consolidation of suspended sediment in a water column (e.g., [59–63]). However, consolidation timespans described may hint towards an ongoing self-weight induced compaction taking place after sampling.

Another successive process eventually leading to higher PR in the future might be internal erosion, more precisely the process of suffusion by seepage leading to clogged pores as described in [64–68]. Within the thoroughly mixed, backfilled material, an interflow- or seepage-driven suffusion of fine particles may most likely occur, as the still present, coarse pumice particles provide wide pores allowing seepage particle transport [69]. In [64], the authors even explicitly discuss the effect of suffusion on PR of Andosols, but they describe the opposite phenomenon, where the upper soil layers lose fine

particles through suffusion. However, they found clear evidence that loss of fine particles reduces PR by destabilizing the soil matrix. Therefore, it seems plausible, that enrichment of fine particles in deeper soil layers leads to the opposite effect. Subject to the condition that a successive downward transport of fine particles will occur in the aftermath of backfilling, CUT EX most likely has not fully consolidated yet and may show higher PR in the future. Ongoing penetrometer measurements of this area are taking place, and further investigations have to clarify if a further consolidation takes place that would explain PR values differing from older backfilled sites.

Trying to isolate major correlations and/or governing factors within the dataset was not as successful as hoped. Concerning correlations, at least general trends were observable. Some of them were expectable, like a positive correlation of depth and PR, others hinted towards the beneficial effects of SOM and SM, as they showed negative correlations.

ANOVA analysis revealed effect sizes merely exceeding small effects according to [52]. Even depth—a factor that should, on first sight, clearly govern PR—showed an effect size of only 0.167. However, this rather surprisingly small effect size is most likely caused by the specific properties of Andosols (undisturbed soils): High sand content and loose soil matrix in unweathered and undisturbed C-Horizons led to less PR-increase with depth, thus not generating a PR increase that would have led to a larger effect size.

Interestingly, ANOVA showed only small effect sizes (0.095 and 0.090) for the factor “area”, even though it was proven that they feature statistically dissimilar datasets. Yet the effect is still significant, albeit small. Larger effect sizes were achieved for the combined factor “(C + Si) and Area”, indicating that disturbance (backfilling) is still one of the main verifiable factors governing PR, as (C + Si) is certainly affected by backfilling, again indicated by homogenized soil textures.

## 5. Conclusions

As one of the first studies published, PR benchmarks for forested Andosol sites were collected. They clearly show undisturbed conditions that may foster root growth and elongation against the background of published critical threshold values. Additionally, effects of pumice excavation and soil backfilling were quantified. On backfilled sites, PR was significantly altered, most likely affecting root growth and elongation. Further studies, partly already conducted and in preparation for publication, have to address two main topics. First of all, a comprehensive analysis of root systems has to be carried out in order to draw conclusions on correlations and dependencies between PR and rooting. Secondly, repeated PR measurements on CUT EX have to be conducted to verify the hypothesis that low PR values are caused by a soil matrix that has not consolidated yet, potentially leading to higher PR in the longer aftermath of backfilling actions. Within this study, the soil physical fundament has been laid for further investigations.

**Author Contributions:** J.J.Z., U.B. conceived and designed the experiments; J.J.Z., U.B., J.D., I.G., R.C.A.H., J.P. and S.S. performed the experiments; J.J.Z., J.D., I.G., R.C.A.H., J.P. and S.S. analyzed the data; J.J.Z., U.B. contributed reagents/materials/analysis tools; J.J.Z. wrote the paper. All authors have read and agreed to the published version of the manuscript.

**Funding:** This research received no external funding.

**Acknowledgments:** We would like to thank Johannes Biwer, forest ranger in the forest district Bendorf and the city of Bendorf, namely mayor Michael Kessler, for allowing and encouraging the investigations. Apart from that, we would like to thank Brigitte Mann for her constant help in the laboratory. In addition, we would like to thank the students of the case study BioGeoWissenschaften 2019, who helped collecting data in the field.

**Conflicts of Interest:** The authors declare no conflict of interest.

## Abbreviations

The following abbreviations are used in this manuscript:

(C + Si)	Clay and silt content
DBD	Soil dry bulk density
LST	Laacher See Tephra
PR	Soil penetration resistance
Q <sub>n</sub>	n-th Quantile
RMSE	Root mean square error
SM	Soil moisture
SOM	Soil organic matter

## References

- Bengough, A.G.; Campbell, D.J.; O'Sullivan, M.F. Penetrometer Techniques in Relation to Soil Compaction and Root Growth. In *Soil and Environmental Analysis: Physical Methods*, 2nd ed.; Smith, K.A., Mullins, C.E., Eds.; Marcel Dekker Inc.: New York, NY, USA, 2000; pp. 377–405.
- Gregory, P.J. *Plant Roots. Growth, activity and interaction with soils*; Blackwell Publishing Ltd.: Oxford, UK, 2006; pp. 145–149.
- Bengough, A.G.; Mullins, C.E. Penetrometer resistance, root penetration resistance and root elongation rate in two sandy loam soils. *Plant Soil* **1991**, *131*, 59–66. [[CrossRef](#)]
- Bengough, A.G.; Mullins, C.E. Mechanical impedance to root growth: a review of experimental techniques and root growth responses. *J. Soil Sci.* **1990**, *41*, 341–358. [[CrossRef](#)]
- Unger, P.W.; Kaspar, T.C. Soil Compaction and Root Growth: A Review. *Agron. J.* **1994**, *86*, 759–766. [[CrossRef](#)]
- Taylor, H.M.; Ratliff, L.F. Root elongation rates of cotton and peanuts as a function of soil strength and soil water content. *Soil Sci.* **1969**, *108*, 113–119. [[CrossRef](#)]
- Ehlers, W.; Köpke, U.; Hesse, F.; Böhm, W. Penetration resistance and root growth of oats in tilled and untilled soil. *Soil Tillage Res.* **1983**, *3*, 261–275. [[CrossRef](#)]
- De Olivera, P.D.; Sato, M.K.; de Lima, H.V.; Rodrigues, S.; da Silva, A.P. Critical limits of the degree of compactness and soil penetration resistance for the soybean crop in N Brazil. *J. Plant Nutr. Soil Sci.* **2016**, *179*, 78–87. [[CrossRef](#)]
- Oleghe, E.; Naveed, M.; Baggs, E.M.; Hallett, P.D. Plant exudates improve the mechanical conditions for root penetration through compacted soils. *Plant Soil* **2017**, *421*, 19–30. [[CrossRef](#)]
- Lampurlanés, J.; Cantero-Martinez, C. Soil Bulk Density and Penetration Resistance under Different Tillage and Crop Management Systems and Their Relationship with Barley Root Growth. *Agron. J.* **2003**, *95*, 526–536. [[CrossRef](#)]
- Materechera, S.A.; Mloza-Banda, H.R. Soil penetration resistance, root growth and yield of maize as influenced by tillage system on ridges in Malawi. *Soil Tillage Res.* **1997**, *41*, 13–24. [[CrossRef](#)]
- Rosolem, C.A.; Foloni, J.S.S.; Tiritan, C.S. Root growth and nutrient accumulation in cover crops as affected by soil compaction. *Soil Tillage Res.* **2002**, *65*, 109–115. [[CrossRef](#)]
- Sinnett, D.; Morgan, G.; Williams, M.; Hutchings, T.R. Soil penetration resistance and tree root development. *Soil Use Manag.* **2008**, *24*, 273280. [[CrossRef](#)]
- Greacen, E.L.; Sands, R.G. Compaction of forest soils: A review. *Aust. J. Soil Sci.* **1980**, *18*, 163–189. [[CrossRef](#)]
- Sands, R.G.; Greacen, E.L.; Gerard, C.J. Compaction of Sandy Soils in Radiata Pine Forests. I. A Penetrometer Study. *Aust. J. Soil Sci.* **1979**, *17*, 101–113. [[CrossRef](#)]
- Sands, R.G.; Bowen, G.D. Compaction of Sandy Soils in Radiata Pine Forests. II. Effects of Compaction on Root Configuration and Growth of Radiata Pine Seedlings. *Aust. For. Res.* **1978**, *8*, 163–170.
- Jakobsen, B.F.; Greacen, E.L. Compaction of Sandy Forest Soils by Forwarder Operations. *Soil Tillage Res.* **1985**, *5*, 55–70. [[CrossRef](#)]
- Kılıç, K.; Özgöz, E.; Akbaş, F. Assessment of spatial variability in penetration resistance as related to some soil physical properties of two fluvents in Turkey. *Soil Tillage Res.* **2004**, *76*, 1–11. [[CrossRef](#)]

19. Alexandrou, A.; Earl, R. The relationships among the pre-compaction stress, volumetric water content and initial dry bulk density of soil. *J. Agric. Eng. Res.* **1998**, *71*, 75–80. [CrossRef]
20. Bennie, A.T.P.; du T. Burger, R. Penetration resistance of fine sandy apedal soils as affected by relative bulk density, water content and texture. *S. Afr. J. Plant Soil* **1988**, *5*, 5–10. [CrossRef]
21. Gerard, C.J. The influence of soil moisture, soil texture, drying conditions and exchangeable cations on soil strength. *Soil Sci. Soc. Am. J.* **1965**, *29*, 641–645. [CrossRef]
22. Mirreh, H.F.; Ketcheson, J.W. Influence of soil bulk density and matric pressure on soil resistance to penetration. *Can. J. Soil Sci.* **1972**, *52*, 477–483. [CrossRef]
23. Payne, D. Soil mechanical properties and root growth. *J. Sci. Food Agric.* **1973**, *25*, 235.
24. Bathke, G.R.; Cassel, D.K.; Hargrove, W.L.; Porter, P.M. Modification of soil physical properties and root growth response. *Soil Sci.* **1992**, *154*, 316–329. [CrossRef]
25. Daddow, R.L.; Warrington, G.E. *Growth-Limiting Soil Bulk Densities as Influenced by Soil Texture*; WSDG Technical Report WSDG-TN-00005; Watershed Systems Development Group, USDA Forest Service: Fort Collins, CO, USA, 1983.
26. O’Connell, D.J. The Measurement of Apparent Specific Gravity of Soils and Its Relationship to Mechanical Composition and Plant Root Growth. In *Soil Physical Conditions and Crop Production*. Ministry of Agriculture, Fisheries, and Food. *Technical Bulletin 29*; H.M.S.O.: London, UK, 1975; pp. 298–313.
27. Schothorst, C.J. *De relatieve dichtheid van zand- en veengrond en zijn betekenis ten aanzien van draagkracht en vochtgehalte volgens een laboratoriumproef*; Instituut voor Cultuurtechniek en Waterhuishouding: Wageningen, The Netherlands, 1963.
28. Eijkelkamp Agrisearch Equipment. *Penetrologger Operating Instructions*; Eijkelkamp: Giesbeek, The Netherlands, 2014. Available online: [https://www.eijkelkamp.com/download.php?file=M10615SAd\\_Penetrologger\\_03ca.pdf](https://www.eijkelkamp.com/download.php?file=M10615SAd_Penetrologger_03ca.pdf) (accessed on 7 January 2020).
29. Baales, M.; Jöris, O.; Street, M.; Bittmann, F.; Weninger, B.; Wiethold, J. Impact of the Late Glacial Eruption of the Laacher See Volcano, Central Rhineland, Germany. *Quart. Res.* **2002**, *58*, 273–288. [CrossRef]
30. Schmincke, H.-U.; Park, C.; Harms, E. Evolution and environmental impacts of the eruption of Laacher See Volcano (Germany) 12,900 a BP. *Quart. Int.* **1999**, *61*, 61–72. [CrossRef]
31. Riede, F.; Bazely, O.; Newton, A.J.; Lane, C.S. A Laacher See-eruption supplement to Tephabase: Investigating distal tephra fallout dynamics. *Quat. Int.* **2011**, *246*, 134–144. [CrossRef]
32. Brauer, A.; Endres, C.; Negendank, J.F.W. Lateglacial calendar year chronology based on annually laminated sediments from Lake Meerfelder Maar, Germany. *Quat. Int.* **1999**, *61*, 17–25. [CrossRef]
33. Bogaard, P.V.D. Ar-40/Ar-39 ages of Sanidine phenocrysts from Laacher-See-tephra (12,900 Yr BP) – chronostratigraphic and petrological significance. *Earth Planet. Sci. Lett.* **1995**, *133*, 163–174. [CrossRef]
34. Kleber, M.; Jahn, R. Andosols and soils with andic properties in the German soil taxonomy. *J. Plant Nutr. Soil Sci.* **2007**, *170*, 317–328. [CrossRef]
35. Rennert, T.; Eusterhues, K.; Hiradate, S.; Breitzke, H.; Buntkowsky, G.; Totsche, K.U.; Mansfeldt, T. Characterisation of Andosols from Laacher See tephra by wet-chemical and spectroscopic techniques (FTIR, 27Al-, 29Si-NMR). *Chem. Geol.* **2014**, *363*, 13–21. [CrossRef]
36. Kleber, M.; Mikutta, C.; Jahn, R. Andosols in Germany—Pedogenesis and properties. *Catena* **2004**, *56*, 67–83. [CrossRef]
37. Zemke, J.J.; Enderling, M.; Klein, A.; Skubski, M. The Influence of Soil Compaction on Runoff Formation. A Case Study Focusing on Skid Trails at Forested Andosol Sites. *Geosciences* **2019**, *9*, 204. [CrossRef]
38. Page-Dumroese, D.; Miller, R.; Mital, J.; McDaniel, P.; Miller, D. *Volcanic-Ash-Derived Forest Soils of the Inland Northwest: Properties and Implications for Management and Restoration*; Rocky Mountain Research Station Proceedings RMRS-P-44; USDA For. Serv.: Fort Collins, CO, USA, 2007.
39. McDaniel, P.A.; Wilson, M.A. Physical and Chemical Characteristics of Ash-influenced Soils of Inland Northwest Forests. In *Volcanic-Ash-Derived Forest Soils of the Inland Northwest: Properties and Implications for Management and Restoration*; Rocky Mountain Research Station Proceedings RMRS-P-44; Page-Dumroese, D., Miller, R., Mital, J., McDaniel, P., Miller, D., Eds.; USDA For. Serv.: Fort Collins, CO, USA, 2007.
40. Kimble, J.M.; Ping, C.L.; Sumner, M.E.; Wilding, L.P. Classification of Soils: Andisols. In *Handbook of Soil Science*; Sumner, M.E., Ed.; CRC Press: New York, NY, USA, 2000.

41. Geist, J.M.; Cochran, P.H. Influences of volcanic ash and pumice deposition on productivity of western interior forest soils. In *Proceedings—Management and Productivity of Western-Montane Forest Soils*; Intermountain Research Station General Technical Report INT-280; Harvey, A.E., Neuenschwander, L.F., Eds.; USDA For. Serv.: Ogden, UT, USA, 1991.
42. Uwitonze, P.; Msanya, B.M.; Mtakwa, P.W.; Uwingabire, S.; Sirikare, S. Pedological Characterization of Soils Developed from Volcanic Parent Materials of Northern Province of Rwanda. *Agric. Fish.* **2016**, *5*, 225–236. [[CrossRef](#)]
43. Ngetich, F.K.; Wandahwa, P.; Wakindiki, I.I.C. Long-term effects of tillage, sub-soiling, and profile strata on properties of a Vitric Andosol in the Kenyan highlands. *J. Trop. Agric.* **2008**, *46*, 13–20.
44. Dörner, J.; Zúniga, F.; López, I. Short-term effects of different pasture improvement treatments on the physical quality of an andisol. *J. Soil Sci. Plant Nutr.* **2013**, *13*, 381–399. [[CrossRef](#)]
45. Dec, D.; Dörner, J.; Balocchi, O.; López, I. Temporal dynamics of hydraulic and mechanical properties of an Andosol under grazing. *Soil Tillage Res.* **2012**, *125*, 44–51. [[CrossRef](#)]
46. Zúniga, F.; Ivelic-Sáez, J.; López, I.; Huygens, D.; Dörner, J. Temporal dynamics of the physical quality of an Andisol under a grazing system subjected to different pasture improvement strategies. *Soil Tillage Res.* **2014**, *145*, 233–241. [[CrossRef](#)]
47. Dörner, J.; Dec, D.; Feest, E.; Vásquez, N.; Díaz, M. Dynamics of soil structure and pore functions of a volcanic ash soil under tillage. *Soil Tillage Res.* **2012**, *125*, 52–60. [[CrossRef](#)]
48. Zemke, J.J.; Pöhler, J.; Stegmann, S. Modeling Runoff-Formation and Soil Erosion after Pumice Excavation at Forested Andosol-Sites in SW-Germany Using WEPP. *Soil Syst.* **2019**, *3*, 48. [[CrossRef](#)]
49. Zaiß, H. *Simulation Ereignisspezifischer Einflüsse des Niederschlag-Abfluss-Prozesses von Hochwasserereignissen Kleiner Einzugsgebiete mit N-A-Modellen*; TH Darmstadt: Darmstadt, Germany, 1989.
50. Schober, P.; Boer, C.; Schwarte, L.A. Correlation Coefficients: Appropriate Use and Interpretation. *Anesth. Analgetica* **2018**, *126*, 1763–1768. [[CrossRef](#)]
51. Overholser, B.R.; Sowinski, K.M. Biostatistics primer: Part 2. *Nutr. Clin. Pract.* **2008**, *23*, 76–84. [[CrossRef](#)]
52. Cohen, J. *Statistical Power Analysis for the Behavioral Sciences*; Taylor and Francis: Milton Park, UK, 1988.
53. United States Department of Agriculture, Agricultural Research Service, Natural Resources Conservation Service, Soil Quality Institute. *Soil Quality Test Kit Guide*; USDA NRCS: Washington, DC, USA, 1999. Available online: [https://www.nrcs.usda.gov/Internet/FSE\\_DOCUMENTS/nrcs142p2\\_050956.pdf](https://www.nrcs.usda.gov/Internet/FSE_DOCUMENTS/nrcs142p2_050956.pdf) (accessed on 19 February 2020).
54. Ampoorter, E.; van Nevel, L.; de Vos, B.; Hermy, M.; Verheyen, K. Assessing the effects of initial soil characteristics, machine mass and traffic intensity on forest soil compaction. *Ecol. Manag.* **2010**, *260*, 1664–1676. [[CrossRef](#)]
55. Franke, J.; Köstner, B.M.M. Effects of recent climate trends on the distribution of potential natural vegetation in Central Germany. *Int. J. Biometeorol.* **2008**, *52*, 139–147. [[CrossRef](#)] [[PubMed](#)]
56. Landesamt für Umwelt, Wasserwirtschaft und Gewerbeaufsicht Rheinland-Pfalz (State Environmental Agency of Rhineland-Palatinate). *Heutige Potentielle Natürliche Vegetation in Rheinland-Pfalz, Karte Bendorf (TK5511)*; Mainz, Germany, 2010. Available online: [https://final.rlp-umwelt.de/download/HpnV/Kartiereinheiten\\_TK25/HPNV\\_Kartiereinheiten\\_5511.pdf](https://final.rlp-umwelt.de/download/HpnV/Kartiereinheiten_TK25/HPNV_Kartiereinheiten_5511.pdf) (accessed on 20 February 2020).
57. Schmid, I.; Kazda, M. Vertical distribution and radial growth of coarse roots in pure and mixed stands of *Fagus sylvatica* and *Picea abies*. *Can. J. Res.* **2001**, *31*, 539–548. [[CrossRef](#)]
58. Coners, H.; Hertel, D.; Leuschner, C. Horizontal- und Vertikalstruktur des Grob- und Feinwurzelsystems von konkurrierenden Buchen und Eichen in einem Mischbestand. *Verh. Ges. Ökol.* **1998**, *28*, 435–440.
59. Wickland, B.E.; Ward Wilson, G. Self-weight consolidation of mixtures of mine waste rock and tailings. *Can. Geotech. J.* **2005**, *42*, 327–339. [[CrossRef](#)]
60. Lee, K.; Sills, G.C. The Consolidation of a Soil Stratum, Including Self-Weight Effects and Large Strains. *Int. J. Numer. Anal. Methods Geomech.* **1981**, *5*, 405–428. [[CrossRef](#)]
61. Been, K.; Sills, G.C. Self-Weight Consolidation of Soft Soils: An Experimental and Theoretical Study. *Geotech* **1981**, *31*, 519–535. [[CrossRef](#)]
62. Lee, K. An Analytical and Experimental Study of Large Strain Soil Consolidation. Ph.D. Thesis, University of Oxford, Oxford, UK, 1979.
63. Terzaghi, K. *Theoretical Soil Mechanics*; Wiley: New York, NY, USA, 1943.

64. Sato, M.; Kuwano, R. Suffusion and clogging by one-dimensional seepage tests on cohesive soil. *Soils Found.* **2015**, *55*, 1427–1440. [[CrossRef](#)]
65. Sherard, J.L.; Dunnigan, L.P.; Talbot, J.R. Filters for silts and clays. *J. Geotech. Eng.* **1984**, *110*, 701–718. [[CrossRef](#)]
66. Sterpi, D. Effects of the Erosion and Transport of Fine Particles due to Seepage Flow. *Int. J. Geomech.* **2003**, *3*, 111–122. [[CrossRef](#)]
67. Chetti, A.; Benamar, A.; Hazzab, A. Modeling of Particle Migration in Porous Media: Application to Soil Suffusion. *Transp. Porous Media* **2016**, *113*, 591–606. [[CrossRef](#)]
68. Idaratna, B.; Nguyen, V.T.; Rujikiatkamjorn, C. Assessing the Potential of Internal Erosion and Suffusion of Granular Soils. *J. Geotech. Geoenviron. Eng.* **2011**, *137*, 550–554. [[CrossRef](#)]
69. Kenny, T.C.; Chahal, E.; Chiu, E.; Ofoegbu, G.I.; Omange, G.N.; Ume, C.A. Controlling constriction sizes of granular filters. *Can. Geotech. J.* **1985**, *22*, 32–33. [[CrossRef](#)]



© 2020 by the authors. Licensee MDPI, Basel, Switzerland. This article is an open access article distributed under the terms and conditions of the Creative Commons Attribution (CC BY) license (<http://creativecommons.org/licenses/by/4.0/>).